1

Chemostratigraphy as a Formal Stratigraphic Method

Alcides Nobrega Sial[1], Claudio Gaucher[2], Muthuvairavasamy Ramkumar[3], and Valderez Pinto Ferreira[1]

ABSTRACT

Elemental and isotope chemostratigraphies are used as tracers for glacial events, buildup of volcanic gases during glaciations (e.g., CO_2), role of volcanism in mass extinction, salinity variation, redox state of the ocean and atmosphere, and provenance, among other applications. The use of isotope systems (C, O, S, N, Sr, Nd, Os), nontraditional stable isotope systems (e.g., Ca, Mg, B, Mo, Fe, Cr, Li), and elemental composition or elemental ratio (e.g., V, Ir, Mo, P, Ni, Cu, Hg, Rb/K, V/Cr, Zr/Ti, Li/Ca, B/Ca, Mg/Ca, I/Ca, Sr/Ca, Mn/Sr, Mo/Al, U/Mo, Th/U) in chemostratigraphy, especially across major chronological boundaries, are reviewed in this chapter. Furthermore, it is discussed what validates chemostratigraphy as a formal stratigraphic method.

1.1. INTRODUCTION

The use of elemental and isotope chemostratigraphy in interpretation and correlation of global events was established with the pioneer work of *Emiliani* [1955] on oxygen isotope composition of foraminifers from deep-sea cores. *Shackleton and Opdyke* [1973] established the first 22 oxygen isotope stages, which was effectively the first formal application of chemostratigraphy. *Williams et al*. [1988] extended the oxygen isotope stage zonation to the rest of the Quaternary and *Lisiecki and Raymo* [2005] to the whole Pliocene. The success of oxygen isotope chemostratigraphy encouraged researchers to use stable isotope stratigraphy in ancient sedimentary successions.

Precambrian chemostratigraphy followed the pioneer research by William T. Holser on ancient ocean water chemistry [*Kaufman et al*., 2007a]. Long-term fluctuations in the chemistry of the seawater have been examined from the C isotope record across thick successions [e.g., *Veizer et al.,* 1980; *Magaritz et al*., 1986], and, in spite of potential effects of late diagenesis on isotope record, important isotope events were demonstrated on a global scale [e.g., *Knoll et al.,* 1986; *Magaritz*, 1989; *Holser*, 1997]. Since then, it became evident that contemporaneous, geographically widely separated marine strata registered similar isotopic compositions. Thereafter, chemostratigraphy became an important technique/tool of intrabasinal and interbasinal stratigraphic correlation to help assemble Precambrian stratigraphic record from fragments preserved in different successions [*Kaufman et al*., 2007b; *Karhu et al.,* 2010; *Sial et al*., 2010a], compensating for poor biostratigraphic resolution of Precambrian fossils [*Veizer et al.,* 1980; *Knoll et al.,* 1986; *Magaritz et al*., 1986; *Knoll and Walter*, 1992; *Kaufman et al.,* 1997; *Corsetti and Kaufman*, 2003; *Halverson et al.,* 2005]. Correlations established through chemostratigraphy can be used to comment on biogeochemical and climate changes through time although the paucity of radiometric constraints on the absolute age of few of the extreme isotope excursions have led to debates on their temporal equivalence [e.g., *Kaufman et al.,* 1997; *Kennedy et al.,* 1998; *Calver et al.,* 2004; *Allen and Etienne*, 2008].

[1] *NEG–LABISE, Department of Geology, Federal University of Pernambuco, Recife, PE, Brazil*

[2] *Instituto de Ciencias Geológicas, Facultad de Ciencias, Universidad de la República, Montevideo, Uruguay*

[3] *Deparment of Geology, Periyar University, Salem, TN, India*

Chemostratigraphy Across Major Chronological Boundaries, Geophysical Monograph 240, First Edition.
Edited by Alcides N. Sial, Claudio Gaucher, Muthuvairavasamy Ramkumar, and Valderez Pinto Ferreira.

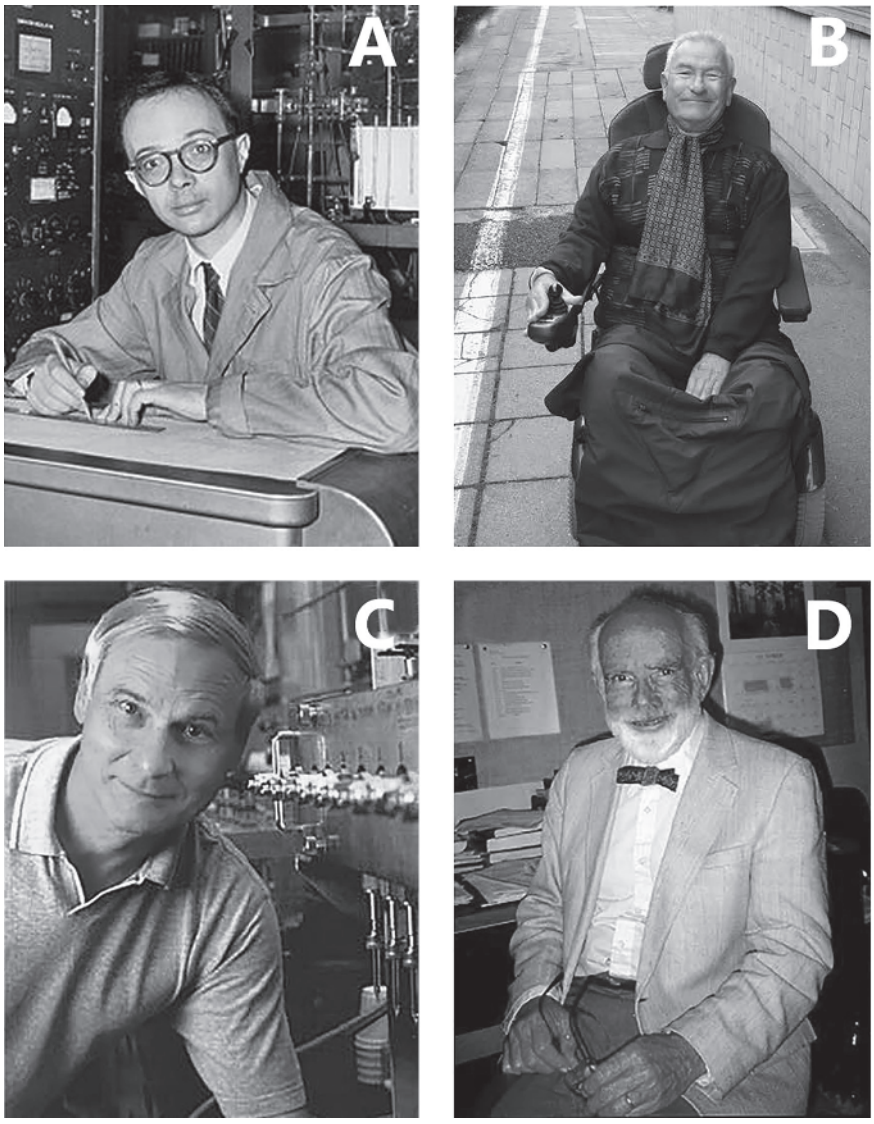

1.2. BASIS AND DEVELOPMENT OF CHEMOSTRATIGRAPHY

High-resolution chemostratigraphy provides records that are multidimensional and that may yield climatic, stratigraphic, biologic, environmental, oceanographic, and, last but not least, tectonic information. Hence, the number of studies relying on isotope stratigraphy has grown substantially. In the case of C isotope stratigraphy, it can be even applied to sedimentary rocks diagenetically altered or that have undergone up to amphibolite facies metamorphism but that may have retained the original isotope signal [*Melezhik et al.,* 2005; *Nascimento et al.,* 2007; *Kaufman et al*., 2007b; *Chiglino et al.,* 2010].

There are a myriad of isotope systems that have been successfully used in chemostratigraphy: carbon, oxygen, sulfur, nitrogen, calcium, boron, chromium, molybdenum, lithium, strontium, neodymium, osmium, iron, and zinc. In order to apply the isotope record of any of these systems for chemostratigraphy of sedimentary sequences, it is essential to have good knowledge of the secular and other variations of marine isotope ratios. As carbon isotopes have higher resilience against postdepositional alteration, they are measured in carbonates and organic matter that led to the establishment of a larger database than other isotope systems. Therefore, $\delta^{13}C$ on carbonates are more widely used in chemostratigraphy, except in carbonate-poor successions characterized by black shales [e.g., *Johnston et al.,* 2010] in which one can measure organic carbon isotopes or carbonate carbon isotopes on fossils (bivalves, ammonites, belemnites, ostracods, etc.). An attempt to compile carbon isotope data to determine a secular variation curve of $\delta^{13}C$ has revealed remarkable $\delta^{13}C$ anomalies in the Proterozoic and Phanerozoic

[e.g., *Veizer et al.,* 1980, 1999; *Karhu and Holland*, 1996; *Hoffman et al.,* 1998b; *Kah et al.,* 1999; *Melezhik et al.,* 1999, 2007; *Zachos et al.,* 2001; *Lindsay and Brasier*, 2002; *Halverson et al.,* 2005, 2010a, 2010b; *Saltzman*, 2005; *Bekker et al.,* 2006; *Saltzman and Thomas*, 2012], and it became apparent that $\delta^{13}C$ minima, perhaps, follow main extinction events [e.g., *Magaritz*, 1989]. The Hirnantian and Frasnian-Famennian episodes, however, are characterized by a positive excursion, and negative excursions are known where extinction was only minor (e.g., early Aptian). A compilation of global secular variation curves of $\delta^{13}C$, $\delta^{18}O$, $\delta^{34}S$, and $^{87}Sr/^{86}Sr$, together with major anoxic events, glaciations, and sea-level variation, can be found in *Sial et al*. [2015a].

The use of chemostratigraphy as a stratigraphic tool requires a careful examination of the diagenetic history of rocks. Petrographic, elemental (e.g., Mn/Sr, Sr, and Rb/Sr vs. $\delta^{13}C$), and isotopic ($\delta^{18}O$ vs. $\delta^{13}C$) proxies are fundamental for the assessment of the nature of C isotope signals [e.g., *Marshall*, 1992; *Jacobsen and Kaufman*, 1999; *Melezhik et al.,* 2001]. In doing so, dolostones and limestones have to be dealt with separately due to their different capacity to retain primary isotopic compositions [e.g., *Kah et al.,* 1999; *Gaucher et al.,* 2007].

Two special issues focusing Precambrian chemostratigraphy were published in *Chemical Geology* [*Kaufman et al*., 2007a] and *Precambrian Research* [*Karhu et al.,* 2010]. In these special issues, results of some cutting-edge research on traditional (C, Sr, S) isotope chemostratigraphy, few nontraditional isotope systems (Ca), and Hg chemostratigraphy have been reported. These publications encompass studies that highlighted chemical events from the Paleoproterozoic (Africa, South America, Europe, and India), Mesoproterozoic (South America), and Cryogenian-Ediacaran (North America, South America, and India) and a special focus to the atmospheric, climatic, and biogeochemical changes in both ends of the Proterozoic eon. In addition, a comprehensive synthesis on the basis and use of chemostratigraphy is presented in the book by *Ramkumar* [2015].

1.2.1. Hydrogen Isotopes

Hydrogen isotopes are relatively little used in chemostratigraphy except in studies of ice and snow stratigraphy, but deuterium has proved to be important isotope in defining the Holocene Global Stratotype Section and Point (GSSP) [*Walker et al.,* 2009]. Quaternary scientists have always sought a boundary stratotype for the Holocene in terrestrial sedimentary records, but it was within the NorthGRIP (NGRIP) ice core, Greenland, that the Holocene GSSP at 1492.45 m depth has been ratified by the International Union of Geological Sciences (IUGS). Physical and chemical parameters within the ice enable the base of the Holocene, marked by the first signs of climatic warming at the end of the Younger Dryas/Greenland Stadial 1 cold phase, located with a high degree of precision [*Walker et al.,* 2009]. This climatic event is reflected in an abrupt shift in deuterium excess values, accompanied by more gradual changes in $\delta^{18}O$, dust concentration, a range of chemical species, and annual layer thickness.

1.2.2. Carbon Isotopes

Carbon isotope investigation on Paleoproterozoic carbonate rocks of the Lomagundi province in Africa revealed much larger $\delta^{13}C$ variation [*Schidlowski et al.,* 1983] than previously known from the Phanerozoic carbonate successions [*Veizer et al.,* 1980]. This observation led to the assumption that $\delta^{13}C$ stratigraphic variation could be a tool in stratigraphic correlation. The pioneer work of *Scholle and Arthur* [1980] is one of the first to use carbon isotopes as stratigraphic tool, and *Berger and Vincent* [1981] recognized chemostratigraphy as a valid stratigraphic method. The potential use of $\delta^{13}C$ trends and excursions of marine carbonates to date and correlate rocks relies on the fact that their $^{13}C/^{12}C$ ratios varied over time as the result of partitioning of carbon between C_{org} and C_{carb} reservoirs in the lithosphere [e.g., *Shackleton and Hall*, 1984; *Berner*, 1990; *Kump and Arthur*, 1999; *Falkowski*, 2003; *Sundquist and Visser*, 2004; *Saltzman and Thomas*, 2012]. The knowledge of the C isotope record is very important not only in stratigraphic correlation but also because of its potential to help understand the development of Earth's climate, evolution of its biota, and CO_2 levels in the atmosphere.

The compilations of the secular $\delta^{13}C_{carb}$ variation for the entire Phanerozoic [*Veizer et al.,* 1999] and the Cenozoic [*Zachos et al.,* 2001] were important steps to enable carbon isotope chemostratigraphy to be routinely used as a stratigraphic tool. Currently, the most complete available curve on the $\delta^{13}C_{carb}$ fluctuations through geologic time has been compiled from multiple literature sources by *Saltzman and Thomas* [2012]. Difficulties faced in constructing such a curve reside on the fact that materials analyzed for curve construction, available in the literature, differ between authors and geological time periods, as cautioned by *Saltzman and Thomas* [2012]. In an attempt to use these compiled curves, one should carefully consider whether skeletal carbonate secreted by specific organisms or bulk carbonate has been used in evaluating or comparing C isotope stratigraphic records. Apparently, the most accepted carbonate $\delta^{13}C_{carb}$ record spanning the Neoproterozoic era is found in *Halverson et al*. [2010a, 2010b].

Covariation between $\delta^{13}C_{carb}$ and $\delta^{13}C_{org}$ helps find out whether variations in the $\delta^{13}C_{carb}$ record reflect changes in

the isotopic composition of the ancient dissolved inorganic carbon (DIC) pool [e.g., *Oehlert and Swart,* 2014]. Covariant $\delta^{13}C_{carb}$ and $\delta^{13}C_{org}$ records attest that both carbonate and organic matter were originally produced in the ocean surface waters and have retained their original $\delta^{13}C$ composition [e.g., *Korte and Kozur*, 2010; *Meyer et al.,* 2013] as no secondary process is able to shift $\delta^{13}C_{carb}$ and $\delta^{13}C_{org}$ in the same direction at the same rate [*Knoll et al.,* 1986]. Conversely, the decoupled $\delta^{13}C_{carb}$ and $\delta^{13}C_{org}$ records point to diagenetic alteration [e.g., *Grotzinger et al.,* 2011; *Meyer et al.,* 2013] or denounce that noise in the $\delta^{13}C_{org}$ record resulted from local syn-sedimentary processes [*Maloof et al.,* 2010]. One should remember, however, that the organic carbon isotope record is very much dependent on the source of the organic matter (terrestrial vs. marine) and terrestrial records may retain the secular variations known from the marine records.

Carbon isotopes can also be used as a pCO_2 proxy. Stratigraphic variation in the offset between the $\delta^{13}C_{carb}$ and $\delta^{13}C_{org}$ expressed by $\Delta^{13}C$ offers a potential tool for tracing paleo-pCO_2 change [*Kump and Arthur*, 1999; *Jarvis et al.,* 2011]. Increased burial of organic carbon leads to a fall in atmospheric pCO_2 and a positive excursion in both inorganic and organic carbon. The peak in $\delta^{13}C_{org}$ may postdate that of inorganic carbon and may be larger in magnitude, because $\Delta^{13}C$ decreases as atmospheric pCO_2 falls. This difference in response is tied to a drawdown in atmospheric pCO_2 [*Kump and Arthur*, 1999]. The "robust voice" of carbon isotopes has the potential to tell us about Earth's history [*Knauth and Kennedy*, 2009], but some postdepositional alteration of carbonate rocks may alter the story [*Bristow and Kennedy*, 2008]. However, indiscriminate use of C isotope stratigraphy to correlate Neoproterozoic carbonates ("blind dating") has been cautioned by *Frimmel* [2008, 2009, 2010] from his studies on REE+Y distribution in Neoproterozoic carbonates from different settings in Africa. These studies have raised some doubt on the usefulness of cap carbonates for stratigraphic correlation of Neoproterozoic sediment successions based on carbon isotopes. They deserve further investigation, although one can argue that rare earth elements (REEs) and DIC behave differently in seawater and are affected by diagenesis in a complete different way.

The application of carbon isotope chemostratigraphy to the study of oceanic anoxic events (OAEs) which record profound global climatic and paleoceanographic changes and disturbance of the carbon cycle, is one of the best examples of use of chemostratigraphy as a stratigraphic tool. The OAEs resulted from abrupt global warming induced by rapid influx of CO_2 into the atmosphere from volcanogenic or methanogenic sources and were accompanied by accelerated hydrological cycle, increased weathering, nutrient discharge to oceans, intensified upwelling, and increase in organic productivity [*Jenkyns*, 2010]. Nine major OAEs are known, the oldest in the Jurassic (Toarcian, called T-OAE, around 183 Ma), seven in the Cretaceous, and the youngest one in the Cenozoic (corresponding to the Paleocene-Eocene Thermal Maximum (PETM), around 55.8 Ma).

An OAE event implies very high burial rates of marine organic carbon (^{12}C), resulting in an increase in $\delta^{13}C$ values of marine and atmospheric carbon, as observed in the pronounced regionally developed positive carbon isotope excursion in $\delta^{13}C_{carb}$ across the Cenomanian-Turonian boundary [*Scholle and Arthur*, 1980]. However, the carbon isotope signatures of the early Toarcian, early Albian, and early Aptian OAEs are more complicated as signals from $\delta^{13}C_{carb}$, $\delta^{13}C_{org}$, and specific biomarkers exhibit both positive and pronounced negative excursions [*Jenkyns and Clayton*, 1986; *Herrle et al*., 2003; *Jenkyns*, 2003, 2010]. This observation suggests that besides carbon burial driving to global $\delta^{13}C$ heavier values, input of light carbon implies movement in the opposite direction.

The selection of a section at El Kef, Tunisia, to be the GSSP for the Cretaceous-Paleogene boundary (K-Pg; 66.02; *Molina et al.,* 2006, 2009), and of one at Dababiya, Egypt, to be the one for the Paleocene-Eocene boundary (PETM; 58.8 ± 0.2 Ma; *Aubry et al.,* 2007), is the best example of use of carbon isotope chemostratigraphy in boundary definition. A $\delta^{13}C$ negative shift in the section at El Kerf was one of the five marker criteria to define the K/Pg boundary, while the Paleocene-Eocene boundary was defined based on global $\delta^{13}C_{org}$ and $\delta^{13}C_{carb}$ isotope excursions (CIE).

1.2.3. Nitrogen Isotopes

The use of $\delta^{15}N$ variations in organic matter (kerogen, $\delta^{15}N_{org}$) has proved to be a valuable tool in the investigation of the evolution of the ocean chemistry, bioproductivity, and chemostratigraphic correlation, especially where biostratigraphy is of limited usefulness [*Beaumont and Robert*, 1999; *Papineau et al.,* 2005; *Algeo et al.,* 2008; *Cremonese et al.,* 2009]. Nitrogen isotope values for bulk samples ($\delta^{15}N_{bulk}$) from sections across the Ediacaran-Cambrian boundary in South China display positive values in the uppermost Ediacaran strata and strong negative shift in the Cambrian strata, especially in black shales, testifying to the changes in the biogeochemical cycle of the ancient ocean [*Cremonese et al.,* 2009, 2013, 2014]. Nitrate and nitrite are reduced to nitrogen gas by denitrification, as part of the global nitrogen cycle in modern oceans [*Algeo et al.,* 2008].

The hypothesis that transition from anoxic to oxygenated deep ocean took place at the end of the Neoproterozoic era (Neoproterozoic Oxygenation Event) is relatively well accepted [e.g., *Canfield et al.,* 2008; *Och and Shields-Zhou*, 2012]. Some of the available geochemical data for

the age interval of this transition, however, allow the interpretation of possibly full oxygenation in the early Ediacaran and preservation of deep ocean anoxia up to as late as the Early Cambrian [*Ader et al.,* 2014].

Changes in marine redox structure are related to changes in the nitrogen nutrient cycling in the global ocean, implying that $\delta^{15}N_{sed}$ probably reflects deep ocean redox transition [*Ader et al.,* 2014]. Nitrogen isotope data from Canada, Svalbard, Amazonia, and China, spanning the 750–580 Ma interval, together with other available $\delta^{15}N_{sed}$ data, show no apparent change between the Cryogenian and Ediacaran, revealing a $\delta^{15}N_{sed}$ distribution that closely resembles modern marine sediments, ranging from −4 to +11, with a $\delta^{15}N$ mode close to +4 [*Ader et al.,* 2014]. $\delta^{15}N$ data from the earlier Proterozoic show distribution relatively similar to this, but shifted slightly toward more negative $\delta^{15}N$ values and with a wider range. A possible explanation for similarity of this $\delta^{15}N$ distributions is that as in the modern ocean, nitrate (and hence O_2) was stable in most of the middle to late Neoproterozoic ocean and possibly much of the Proterozoic eon [*Ader et al.,* 2014].

Global climate over Quaternary glacial-interglacial time scales may have affected fluctuations of denitrification intensity whose rates varied over time, especially during OAEs (e.g., T-OAE; *Jenkyns et al.,* 2001). Some Upper Carboniferous black shales display C_{org}/N ratios and nitrogen isotope data that attest to fluctuations in the intensity of denitrification associated with glacially driven sea-level changes [*Algeo et al.,* 2008]. Sedimentary $\delta^{15}N$ increases during rapid sea-level rise in each cycle, with intensified denitrification, returning to background levels as sea level stabilized during the interglacial phase.

Bulk $^{15}N_{tot}$ data from early Toarcian black carbon-rich shales from British Isles and northern Italy (T-OAE; *Jenkyns et al.,* 2001, 2010) and from the Toarcian-Turonian OAE [*Jenkyns et al*., 2007] have revealed a pronounced positive $\delta^{15}N_{tot}$ excursion that broadly correlates with a relative maximum in weight percent TOC and, in some sections, with a negative $\delta^{13}C_{org}$ excursion. Perhaps, the upwelling of a partially denitrified, oxygenated water mass is the explanation for the relative enrichment of $\delta^{15}N_{tot}$, and the development of early Toarcian suboxic water masses and partial denitrification is attributed to increases in organic productivity [*Jenkyns et al.,* 2001]. A negative $\delta^{15}N_{org}$ peak to near 0‰ air/N_2 occurs at the Permian-Triassic (P-T) boundary parallel to a negative $\delta^{13}C$ excursion. It has been interpreted as the result of a diminished biomass of eukaryotic algae due to mass extinction, which were replaced by microbial N_2 fixers such as cyanobacteria [*Fio et al.,* 2010]. An analogous negative $\delta^{15}N_{org}$ and $\delta^{15}N_{bulk}$ excursion has been reported from the Ordovician-Silurian boundary [*Luo et al.,* 2016] and from the Ediacaran-Cambrian boundary [*Kikumoto et al.,* 2014]. Thus, nitrogen isotopes are valuable for the definition of major chronostratigraphic boundaries.

1.2.4. Oxygen Isotopes

Oxygen isotope chemostratigraphy has become an important tool for Mesozoic and Cenozoic stratigraphic correlation of marine sediments [e.g., *Friedrich et al.,* 2012]. For such studies, $\delta^{18}O$ is usually measured on benthic foraminifera to avoid isotopic gradient effects [e.g., *Emiliani*, 1955; *Shackleton and Opdyke*, 1973; *Lisiecki and Raymo*, 2005]. The demonstration of primary nature of $\delta^{18}O$ values in older successions, however, is often difficult, although oxygen isotopes have been successfully used in carbonates from belemnites and brachiopods and phosphates from shark teeth and conodonts [e.g., *Vennemann and Hegner*, 1998; *Joachimski and Buggisch*, 2002; *Puceat et al.,* 2003; *Price and Mutterlose*, 2004; *Bodin et al.,* 2009; *Dera et al.,* 2009; *Van de Schootbrugge et al.,* 2013].

Oxygen isotope ratios in foraminifera from deep-sea cores have shown a consistent pattern representing changes in the ocean-atmosphere system through time. *Emiliani* [1955], based on the major swings in his data, has recognized the "marine isotope stages" (MIS). *Shackleton* [1969] has subdivided Emiliani's stage 5 into lettered substages, and since then, Quaternary time is divided into marine isotope stages and substages. The MIS scheme was the first attempt to use oxygen isotope chemostratigraphy in the Quaternary. *Railsback et al*. [2015] have proposed the scheme of marine isotope substages currently in use.

A general increase from −8 to 0‰ VPDB in the Phanerozoic, punctuated by positive excursions coincident with cold intervals, has been recognized by *Veizer et al*. [1999] who have suggested that $\delta^{18}O$ analyses of carefully screened, well-preserved brachiopods and mollusks can still retain a primary signal even in Paleozoic samples. Nevertheless, similar consideration is not possible for the Precambrian due to the absence of calcified metazoans, except for the Ediacaran. $\delta^{18}O$ analyses of whole rock samples of Precambrian successions usually reflect diagenetic conditions, although primary trends have been reported in rare/limited occasions [Tahata *et al.,* 2012].

According to *Bao et al*. [2008, 2009], triple oxygen isotope evidence proved to be an important tool in the discrimination of early-Cryogenian from end-Cryogenian cap carbonates. Sulfate from ancient evaporites and barite shows variable negative ^{17}O isotope anomalies over the past 750 million years. An important difference in ^{17}O isotope anomalies of barite at top of the dolostones from the Marinoan cap carbonates (negative spike ~ −0.70‰) suggests that by the time this mineral was precipitated, P_{CO2} was highest for the past 750 million years (CO_2 levels reached 0.01–0.08 bar during and just after ~635 Ma glacial event; *Bao et al.,* 2008, 2009].

Oxygen isotopes of dissolved inorganic phosphate (δ^{18}Op) are a powerful stable isotope tracer for biogeochemical research, offering insights into the relative importance of different sources of phosphorus within natural ecosystems [*Davies et al.,* 2014]. Besides, the isotope fractionations alongside the metabolism of phosphorus allow δ^{18}Op to be used to better understand intracellular/extracellular reaction mechanisms that control phosphorus cycling.

An organic paleothermometer based upon the membrane lipids of mesophilic marine Thaumarchaeota, the tetraether index of lipids, with 86 carbon atoms (TEX86) has been used for over a decade when attempting to reconstruct sea surface temperatures (SSTs). This thermometer is particularly useful when other SST proxies are diagenetically altered (e.g., planktic foraminifera; *Pearson et al.,* 2007) or absent (e.g., alkenones; *Bijl et al.,* 2009).

The oldest TEX_{86} record is from the Middle Jurassic (~160Ma) and indicates relatively warm SST [*Jenkyns et al.,* 2012]. It has been also used to reconstruct SST throughout the Cenozoic era (66–0 Ma) [e.g., *Sluijs et al.,* 2009; *Zachos et al.,* 2006] and particularly to reconstruct the Eocene (55.8–34 Ma) SST. During the early Eocene, TEX_{86} values indicate warm high southern hemisphere latitude SSTs (20–25 °C) in agreement with other independently derived proxies (e.g., alkenones, Mg/Ca). During the middle and late Eocene, high southern latitude sites cooled, while the tropics remained stable and warm.

The field of clumped isotopes is concerned with how the various isotopes of carbon and oxygen are distributed in the lattice of the carbonate crystal, allowing distinction of the "isotopologues," that is, molecules of similar chemical composition but different isotopic composition [*Eiler*, 2007]. This field is concerned with measuring an isotopologue of CO_2 gas with a mass of 47, that is, where the two "heavy" rare isotopes (^{13}C and ^{18}O) are substituted in the CO_2 molecule. This is representative of the amount of "clumping" of the heavy isotopes in the crystal lattice of the carbonate. As $\Delta 47$ is measured, the amount of clumping at a known temperature can be determined [e.g., *Ghosh et al.,* 2006]. *Guo et al*. (2009b) provided a theoretical Δ_{47} calibration for a number of different mineralogies, making clumped isotopes to be one of the most promising paleothermometer for paleoclimate and diagenesis [e.g., *Eagle et al.,* 2010; *Tripati et al.,* 2010; *Petrizzo et al.,* 2014]. The great advantage is that it is unnecessary to know the oxygen isotope composition of the water with which carbonates have isotopically equilibrated. The growing interest on use of this technique is reflected in a rapid increase in the number of laboratories equipped to perform routine analyses of clumped isotope and by the organization of a series of international workshops focusing on its development and general applications.

1.2.5. Sulfur Isotopes

A secular δ^{34}S variation curve for evaporites (1.0 Ga to present) was reported by *Claypool et al*. [1980], and since then sulfur isotope chemostratigraphy has been largely used for marine evaporite sulfate, in terrains ranging from 1.0 Ga to recent. Extensive critical review on sedimentary sulfur through time and on potential use of sulfur isotopes in the investigation of time boundaries is found in *Strauss* [1997], while detailed discussion on the use of sulfur isotopes on Neoproterozoic chemostratigraphy can be found in *Halverson et al*. [2010a]. *Halverson et al*. [2010b] have subdivided Neoproterozoic sulfur isotope data into two kinds: one recording seawater sulfate ($\delta^{34}S_{sulph}$) and the other recording epigenic or authigenic pyrite ($\delta^{34}S_{pyr}$). The former is recovered from evaporites, barites, phosphorites, and carbonates (as carbonate-associated sulfate (CAS)). Fractionation that occurs during bacterial sulfate reduction (BSR) plus additional fractionation effects of reactions during oxidative recycling of sulfides is recorded by the pyrite data [*Canfield and Teske*, 1996], while the sulfur isotope data from barite, phosphorite, and CAS depict seawater sulfate ($\delta^{34}S_{sulph}$). Due to BSR, $\delta^{34}S_{pyr}$ is usually lower (lighter) than $\delta^{34}S_{sulph}$. Two important exceptions to this rule have been reported [*Ries et al.,* 2009]: (i) Archean successions usually yield similar values for pyrite and CAS, because the ocean was anoxic, and therefore BSR was negligible. (ii) Superheavy pyrites, that is, with δ^{34}S values exceeding that of coeval sulfides, occur in late Neoproterozoic successions and were interpreted as the result of very low sulfate concentrations and ferruginous conditions in the ocean and intense aerobic reoxidation of pyrite [*Ries et al.,* 2009].

Mass-independent fractionation (MIF) is observed in O, S, and Hg, linked to photochemical reactions in the atmosphere, and in the case of sulfur, it can be observed in ancient sediments [*Farquhar et al.,* 2000; *Guo et al*., 2009b] where it preserves a signal of the prevailing environmental conditions which makes sulfur isotopes as a tracer of early atmospheric oxygenation up to the formation of the ozone shield. The method implies measurements of multiple sulfur isotopes (δ^{33}S, δ^{34}S, and δ^{36}S) on CAS and sulfides. The creation and transfer of the mass-independent (MI) signature into minerals would be unlikely in an atmosphere containing abundant oxygen, constraining the Great Oxygenation Event (GOE) and the establishment of an ozone shield to sometime after 2.45 Ga ago. Prior to this time, the MI sulfur record implies that sulfate-reducing bacteria did not play a significant role in the global sulfur cycle and that the MI sulfur signal is due primarily to changes in volcanic activity [*Halevy et al.,* 2010]. After 2.3 Ga, the MIF signal disappears, attesting to the continued existence of an ozone layer since the Paleoproterozoic [*Guo et al*., 2009a].

Therefore, sulfur isotopes are important in the study of the Archean-Paleoproterozoic boundary and the fundamental biotic and environmental changes that took place during the GOE.

Biological and abiotic reactions in the sulfur biogeochemical cycle show distinctive stable isotopic fractionation and are important in regulating the Earth's surface redox state [*Pasquier et al.,* 2017]. The $\delta^{34}S$ composition of sedimentary sulfate-bearing phases reflects temporal changes in the global sulfur cycle and can be used to infer major changes in the Earth's surface environment, including rise of atmospheric oxygen.

Sulfur isotope pyrite-based records have been less explored. *Pasquier et al*. [2017] have studied Mediterranean sediments deposited over 500,000 y which exhibit stratigraphic variations >76‰ in the $\delta^{34}S$pyr data. These authors have demonstrated the relationship between the stratigraphic isotopic variation and phases of glacial-interglacial sedimentation rates. Their results suggest that the control of the sulfur isotope record can be associated with strong sea-level variations. Besides, they provided an important perspective on the origin of variability in such records and suggested that meaningful paleoenvironmental information can be derived from pyrite $\delta^{34}S$ records.

1.2.6. Calcium, Magnesium, and Boron Isotopes

Technological advances in analytical procedures and sophistication of equipment (e.g., micro-SIMS, nano-SIMS, MC-ICPMS) for few nontraditional stable isotopes, mainly Li, B, Mg, Cl, Ca, Cr, Fe, Ni, Cu, Zn, Ge, Se, Mo, Os, Hg, and Th [*Johnson et al.,* 2004; *Baskaran*, 2012; *Teng et al.,* 2017], have opened new avenues, some still to be explored in terms of isotope chemostratigraphy. In particular, Ca, Mo, and Fe have received more attention in Precambrian isotope chemostratigraphy [*Kasemann et al.,* 2005; *Arnold et al.,* 2004; *Siebert et al.,* 2003; *Johnson and Beard*, 2006; *Staubwasser et al.,* 2006, among others], and Cr isotopes have proven to be an important tool in this regard [*Frei et al.,* 2009, 2011, among others].

It is not known exactly how Ca isotopes work in modern carbonate rocks or the extension on how diagenesis affects them. A fairly updated review on the global calcium cycle is found in *Fantle and Tipper* [2014] and *Gussone et al*. [2016].

The global Ca isotope signal from end-Cryogenian carbonate successions suggests that Ca isotope chemostratigraphy can be an additional tool for the correlation of postglacial Neoproterozoic carbonate successions [*Higgins and Schrag*, 2010; *Kasemann et al.,* 2005; *Silva Tamayo et al*., 2007, 2010a, 2010b]. These authors have claimed that the Neoproterozoic Ca isotopic record is, perhaps, an archive of changes in the oceanic Ca isotopic composition.

Rapid glacier melting and significant increase in the Ca input to the ocean immediately after deglaciation, followed by progressive increase in carbonate precipitation and burial compensating for the large initial Ca input, have been depicted from Ca isotope behavior. Post-Sturtian and post-Marinoan global $\delta^{44/40}Ca$ patterns seem to differ from each other, probably because of the difference in Ca mass balance evolution among these two deglaciation events as a consequence of contrasting glacier melting regimes [*Silva Tamayo et al*., 2010a, 2010b]. This divergent behavior of the Ca isotopic evolution makes Ca isotope stratigraphy a promise, perhaps, to discriminate and correlate Neoproterozoic postglacial carbonate successions. Possibly, there is a close connection between Ca isotopic cycling in the Phanerozoic, seawater chemistry, carbonate sedimentation, and evolutionary trends [*Blättler et al.,* 2012]. MI isotope fractionation effects as observed in O, S, and Hg isotopes were not so far observed in Ca isotopes [*Gussone et al.,* 2016].

Use of magnesium isotope to understand geological phenomenon/processes has been on the rise during recent times [e.g., *Tipper et al.,* 2006a, 2006b, 2006c; *Higgins and Schrag*, 2010; *Wombacher et al.,* 2011; *Azmy et al.,* 2013; *Geske et al.,* 2015]. *Chang et al*. [2003], *Tipper et al*. [2008], and *Wombacher et al*. (2009) presented the systematics and analytical protocols in Mg isotope analyses, and accuracy of Mg isotope determination in MC-ICPMS was discussed by *Tipper et al*. [2008]. *Brenot et al*. (2008) examined the Mg isotope variability within a lithologically diverse river basin. The relationships between continental weathering, riverine influx of Mg into the oceans, and global Mg isotope budgets of modern oceans were examined by *Tipper et al*. [2006a, 2006b, 2006c]. *Higgins and Schrag* [2010] demonstrated the utility of constraining Mg cycle in marine sediments through the use of Mg isotope. As magnesium is part of the C cycle and dolomite is a major sink for Mg and a main control for $\delta^{26}Mg_{seawater}$, *Geske et al*. [2015] studied Mg isotope and suggested its use as a vital proxy. *Azmy et al*. [2013] are also of the similar opinion. Nevertheless, use of Mg isotopes in truly stratigraphic context has been scarce, for example, *Strandmann et al*. [2014] and *Pokrovsky et al*. [2011], to name a few. Despite this scarcity, the information that the Mg isotope system follows that of Sr and Ca isotopic systems [*Fantle and Tipper*, 2014] and the fact that the Mg isotopic composition of the oceans is relatively constant ($\delta^{26}Mg_{seawater} = -0.82 \pm 0.01$‰, *Foster et al.,* 2010) and Mg has a long residence time in the ocean (≈10 Myr; *Berner and Berner*, 1987; 14–16 Myr, *Lécuyer et al.,* 1990) could suggest its utility in establishing chemostratigraphic curve similar to that of Sr isotopic curve; however, the potential remains yet to be tapped and tested. It was *Galy et al*. [2002] who have reported a latitudinal gradient of Mg isotopic fractionation in

calcites of speleothems. *Li et al*. [2012] precipitated calcite in a wide range of temperature (4–45 °C) and reported a feeble gradient between $\delta^{26}Mg_{\text{calcite in solution}}$ and temperature (0.011 ± 0.002‰ $°C^{-1}$). This finding could help establish Mg isotope as a proxy to temporal trends of paleotemperature and paleolatitudinal variations.

There is fair agreement on that the aftermath of the Cryogenian glaciations has been marked by cap dolostone deposition that have followed intense continental chemical weathering. *Huang et al*. [2016] have explored the behavior of Mg isotopes to demonstrate that this was the picture in the deposition of the terminal Cryogenian-age Nantuo Formation and the overlying cap carbonate of the basal Doushantuo Formation, South China. They observed a δ^{26}Mg positive excursion, with values ranging from +0.56 to +0.95‰, in the top of the Nantuo Formation that likely resulted from an episode of intense chemical weathering. The siliciclastic component of the overlying Doushantuo cap carbonate, on the contrary, has yielded much lower δ^{26}Mg values (<+0.40‰), suggesting low-intensity chemical weathering during the cap carbonate deposition. *Huang et al*. [2016] concluded that such a behavior of Mg isotopes confirms an intense chemical weathering at the onset of deglaciation and that it has reached its maximum before the cap carbonate deposition.

There are a growing number of publications that have applied boron isotopes as a paleo-pH proxy although boron isotope analyses are complex [e.g., *Palmer et al.,* 1998; *Sanyal et al*., 2001; *Joachimski et al.,* 2005; *Hemming and Hönisch*, 2007; *Hönisch et al*., 2012; *Foster and Rae*, 2016]. A secular change in the boron isotope geochemistry of seawater over the Phanerozoic is found in *Joachimski et al*. [2005], based on the boron isotope geochemistry of brachiopod calcite.

It is known that oceanic uptake of CO_2 decreases ocean pH [*Kasemann et al.,* 2005]. Calcium and boron isotopes have been used to estimate paleoenvironmental conditions in the aftermath of the two major Neoproterozoic glaciations in Namibia. *Kasemann et al*. [2005] presented a record of Cryogenian interglacial ocean pH based on boron isotopes in marine carbonates. Their B isotope data suggest a largely constant ocean pH and no critically elevated pCO_2 throughout the older postglacial and interglacial periods. Marked ocean acidification event, in contrast, marks the younger deglaciation period and is compatible with elevated postglacial pCO_2 concentration. Negative δ^{11}B excursions in postglacial carbonates have been interpreted as an indication of temporary decrease in seawater pH.

It has been proposed that during the PETM, thousands of petagrams of carbon (Pg C) were released as methane or CO_2 into the ocean-atmosphere system for about 10 kyr, concomitant to a carbon isotope excursion, widespread dissolution of deep-sea carbonates, and global warming, leading to possible severe acidification of the ocean surface [*Penman et al.,* 2014]. Using boron-based proxies for ocean carbonate chemistry, these authors demonstrated that there is evidence for a pH drop of surface and seawater thermocline during the PETM. They have observed a decrease of 0.8‰ in δ^{11}B at the onset of the PETM event and a reduction of almost 40% in shell B/Ca, at a drill site in the North Pacific and similar trends in the South Atlantic and Equatorial Pacific, consistent with global acidification of the surface of the ocean.

1.2.7. Chromium, Iron, Molybdenum, and Thallium Isotopes

Widespread deepwater anoxia predominated in the Archean and Paleoproterozoic oceans, while the Neoproterozoic was transitional between anoxic and largely oxygenated Phanerozoic oceans. Stratified, ferruginous oceans have characterized the Archean-Paleoproterozoic and Neoproterozoic ocean chemistries, while during the Mesoproterozoic, sulfidic (euxinic) marine conditions prevailed in contrast with Phanerozoic oxygenated conditions [*Canfield et al.,* 2008]. Investigation on the Fe, Cr, and Mo isotope behavior has provided further insights into the question of surface ocean oxygenation [*Scott et al.,* 2008; *Frei et al.,* 2009].

It is well known that Cr is very sensitive to the redox state of the surface environment, oxidative weathering processes producing the oxidized hexavalent Cr. Positive isotopic fractionation of up to 5‰ accompanies the oxidation of the reduced Cr(III) on land [*Frei et al.,* 2009 and references therein]. *Lyons and Reinhard* [2009] and *Døssing et al*. [2011] have discussed in detail the isotopic systematic of the Cr cycle, including incorporation into banded iron formation (BIF). From Cr isotopes in BIFs, one can track the presence of hexavalent Cr in Precambrian oceans to understand the oxygenation history of the Earth's atmosphere-hydrosphere system [*Frei et al.,* 2009]. *Frei et al*. [2011] applied for the first time Cr isotope systematics to ancient carbonates, representing a useful tracer for climate change and for reconstructing the redox state of ancient seawater and atmosphere. Cr and C isotope curves in carbonates are virtually parallel [*Frei et al.,* 2011], and therefore, coupled δ^{13}C-δ^{53}Cr chemostratigraphy of mixed BIF/carbonate/chert successions may provide more continuous curves than C isotopes alone. This method is suitable for chemical sediments (BIF, chert, and carbonates), with low amounts of terrigenous material; otherwise Cr isotopic composition of the rock will predominate [*Frei et al.,* 2013]. Cr isotopes enabled the detection of early oxygenation pulses at 2.7 Ga [*Frei et al.,* 2009] and even at 2.95 Ga [*Crowe et al.,* 2013], long before the GOE. If one compares the δ^{53}Cr

values of BIF of different ages, Archean BIFs are the less fractionated and Neoproterozoic BIFs show the largest positive values, in accordance with the progressive oxygenation of surface environments [*Frei et al.,* 2009, 2013, 2017].

Iron (Fe) isotopes are a tool in the study of iron cycling due to its large isotopic fractionation attending to redox transformations in near-surface environment. Before the impossibility of applying the traditional stable or radiogenic isotope systems, the Fe isotope system has been largely applied to BIF [*Halverson et al.,* 2011]. Archean and Paleoproterozoic BIFs have revealed an extraordinary variability in Fe isotope compositions, from the stratigraphic [e.g., *Beard et al.,* 2003; *Johnson et al.,* 2008; *Heimann et al.,* 2010] to the mineral [e.g., *Johnson et al.,* 2003; *Frost et al.,* 2007] and microscale [e.g., *Steinhoefel et al.,* 2010]. These variations are usually ascribed to the large fractionation resulting from reduction/oxidation of Fe and the isotopic differences between mineral phases [e.g., *Johnson et al.,* 2008].

In Neoproterozoic iron formations (IF), Fe occurs almost predominantly as hematite [*Klein and Beukes*, 1993] in contrast to some Archean-Paleoproterozoic BIFs in which iron occurs as both Fe^{2+} and Fe^{3+} in a range of different minerals [*Klein and Beukes*, 1993]. Therefore, primary isotope signatures are easier to obtain from the Neoproterozoic BIFs which are usually associated with episodes of global glaciation (Rapitan-type BIF) as their Fe isotope composition reflects the chemistry of the glacial ocean [*Halverson et al.,* 2011].

The evolution of the redox state of the oceans can be also investigated using Mo concentrations in black shales [*Scott et al.,* 2008]. Its isotopic composition, in turn, allows differentiation between euxinic (i.e., sulfidic) and oxygenated environments [*Arnold et al.,* 2004]. Three oxygenation events at 2.65 Ga, ca. 2.5 Ga, and 550 Ma were recognized, with the late Paleoproterozoic and Mesoproterozoic (1.8–1.0 Ga) being characterized by euxinic conditions ("Canfield Ocean"; *Canfield*, 1998; *Arnold et al.,* 2004; *Scott et al.,* 2008). This is consistent with other proxies, such as MIF of sulfur and chromium isotopes.

High-precision measurements of thallium (Tl) isotope ratios were only made possible in the late 1990s, and, therefore, one has only limited knowledge of its isotopic behavior. Despite of their heavy masses of 203 and 205 a.m.u., it is known that thallium isotopes can be fractionated substantially in the marine environment [*Nielsen et al.,* 2017].

Thallium isotopes have been applied to investigate paleoceanographic processes in the Cenozoic, and a compilation of the Tl ($\varepsilon^{205}Tl_{sw}$) isotope composition of seawater over the last 75 Myrs is found in *Nielsen et al*. [2009, 2017], together with contemporaneous $\delta^{34}S_{sw}$ variation curve. These two curves show relatively similar behavior, with the lowest values within the 55–70 Ma range, the $\delta^{34}S_{sw}$ curve displaying minimum values around 55 Ma and $\varepsilon^{205}Tl_{sw}$ around 66 Ma. Thallium isotopes may be utilized as a proxy for changes in Fe and Mn supply to the water column over million year time scales according to *Nielsen and Rehkämper* [2012] to monitor changes in marine Mn sources and/or Mn oxide precipitation rates back in time.

1.2.8. Strontium and Neodymium Isotopes

As $^{87}Sr/^{86}Sr$ ratios and $\delta^{13}C$ fluctuate independently from each other, their combined use through the application of high-resolution chemostratigraphy represents a powerful tool to resolve geological problems. The radiogenic nature of ^{87}Sr, which forms as a result of radioactive decay of ^{87}Rb, implies that the $^{87}Sr/^{86}Sr$ ratio of the mantle, crust, and surface environments rises with time [e.g., *Shields,* 2007a, 2007b]. The $^{87}Sr/^{86}Sr$ seawater variation curve is better known for the Phanerozoic [e.g., *Burke et al.,* 1982; *Veizer et al.,* 1999; *McArthur et al.,* 2001; *Leckie et al.,* 2002; *McArthur*, 2010] showing long-term variations of about 500–550 Ma from the Upper Cambrian (0.709; *Montañez et al.,* 2000) gradually decreasing with a nadir of 0.7068 at 250 Ma and rising again to values of 0.7092 in the present-day ocean [*Macdougall*, 1991; *McArthur et al.,* 2001]. This makes Sr isotopes a pretty straightforward and precise method for dating marine carbonates and calcareous fossils in the upper half of the Cenozoic, for example, because $^{87}Sr/^{86}Sr$ ratios rise continuously from 0.7077 in the Bartonian (ca. 40 Ma) to 0.7092 in the Holocene [*McArthur et al.,* 2001]. Sr isotope chemostratigraphy is equally well feasible in the other periods of the Phanerozoic, depending on the morphology of the Sr isotope record. The close correlation in time between the strontium isotope excursions and the major OAEs (Jurassic and Cretaceous) is compatible with a causal linkage [e.g., *Jones and Jenkyns*, 2001].

The main source of ^{87}Sr is the weathering of Rb-rich granitic rocks. Hydrothermal vents near mid-ocean ridges are enriched in non-radiogenic ^{86}Sr [*Shields*, 2007a], and therefore, high $^{87}Sr/^{86}Sr$ ratios are considered as an indication of periods of enhanced orogenesis, while low ratios characterize periods of continental breakup and enhanced hydrothermal activity. *Flament et al*. [2011], however, have pointed out that $^{87}Sr/^{86}Sr$ is influenced by the area of emerged land rather than by orogenic processes alone, something especially important for calculations of continental growth in the Archean, when maybe <4% of Earth's area was emerged [*Shields*, 2007b; *Flament et al.,* 2011].

Efforts to compile Sr isotope data aimed at determining the secular $^{87}Sr/^{86}Sr$ seawater curve for the Proterozoic have been made [e.g., *Jacobsen and Kaufman*, 1999;

Melezhik et al., 2001; *Halverson et al*., 2007, 2010a, 2010b; *Kuznetsov et al.,* 2010]. The use of strontium isotopes in chemostratigraphy, however, is limited by the paucity of limestone in many successions. Another difficulty is posed by the likelihood of alteration in samples with low strontium contents through the incorporation of ^{87}Sr from the decay of ^{87}Rb in coexisting clay minerals [*Kaufman et al.,* 2009]. Therefore, it is advisable to consider only analyses of high-Sr limestones, less prone to postdepositional alteration. Geochemical screens (Rb/Sr, Mn/Sr, Sr concentration, and $\delta^{18}O$) have been widely adopted to evaluate the degree of postdepositional alteration of strontium isotope ratios [*Veizer et al.,* 1983; *Kaufman et al*., 1992, 1993; *Marshall*, 1992; *Jacobsen and Kaufman*, 1999; *Melezhik et al.,* 2001]. Dolostones are usually not suitable for Sr isotope studies due to the lower Sr concentrations of usually a few tens of ppm [*Kah et al.,* 1999; *Gaucher et al.,* 2007], although a few exceptions have been reported [*Sawaki et al.,* 2010].

Another problem of the method is the differing laboratory procedures, which yield different results for the same samples. The use of pre-leaching with ammonium acetate removes adsorbed Sr and yields lower $^{87}Sr/^{86}Sr$ ratios than a more aggressive one-step HCl leaching method [*Melezhik et al.,* 2001; *Rodler et al.,* 2017]. An intermediate approach for limestones is the use of 0.5 M acetic acid for a short time (5–10 min), which predominantly liberates calcite-associated Sr, thereby yielding lower Sr isotope ratios [e.g., *Frei et al.,* 2011].

Details on the neodymium isotope geochemistry are found in *DePaolo* [1988]. A "global average" εNd curve for the oceans since 800 Ma has been constructed [*Keto and Jacobsen*, 1988; *Macdougall*, 1991], although neodymium isotopes have been seldom used as a chemostratigraphic tool. Similar to Sr isotope secular curve, this curve shows ε_{Nd} values at the end of the Precambrian oceans not substantially different from those at present ones. There is a remarkable decrease of the average ε_{Nd} values (−5 to −15) in the time interval between 700 and 550 Ma. Despite the precision of modern instruments, the scatter in measured values is substantial, limiting the use of ε_{Nd} in chemostratigraphic studies. Even so, secular ε_{Nd} variations coupled with $\delta^{13}C$ and $\delta^{53}Cr$ have been reported from Ediacaran rocks from Uruguay [*Frei et al.,* 2011, 2013] and Brazil [*Dantas et al.,* 2009], yielding valuable information regarding the tectonic evolution of the basin.

1.2.9. Osmium and Lithium Isotopes

The temporal variations of the $^{187}Os/^{188}Os$ ratio are preserved in several marine depositional environments, where osmium is an ultra trace element [*Peckeur-Ehrenbrink and Ravizza,* 2000]. Several developments over the last three decades have allowed direct measuring of $^{187}Os/^{188}Os$ ratio and osmium concentration in seawater, river water, and rain, improving the knowledge on the surficial cycle of osmium [*Sharma et al.,* 1997; *Peckeur-Ehrenbrink and Ravizza,* 2000]. *Ravizza and Peucker-Ehrenbrink* [2003] have observed a decline of about 25% in the marine $^{187}Os/^{188}Os$ record that predated the Cretaceous-Paleocene transition (K-Pg) and that coincides with a warming in the late Maastrichtian. They have interpreted this osmium isotope ratio decline as a chemostratigraphic marker of the Deccan volcanism which was responsible for a transient global warming event (3–5 °C) and likely one of the causes of the K-Pg mass extinction.

Precambrian-to-Pleistocene marine osmium isotope records, particularly the Cenozoic and Mesozoic ones, and interpretations of their temporal variations have been reviewed by *Peckeur-Ehrenbrink and Ravizza* [2012]. Although the Cenozoic seawater $^{187}Os/^{188}Os$ mimics the marine $^{87}Sr/^{86}Sr$ record and suggests that both reflect continental weathering linked to climatic or tectonic processes, these two marine isotope systems differ fundamentally from each other [*Peckeur-Ehrenbrink and Ravizza,* 2000]. The marine residence time of osmium is distinctly shorter, allowing to record short-term fluctuations (e.g., glacial-interglacial periods), something that escapes to the buffered marine strontium isotope system. This difference between these two systems allows discrimination between climatic and tectonic forcings. Besides, large-amplitude changes in the marine $^{187}Os/^{188}Os$ record can be useful as chemostratigraphic event markers [*Peckeur-Ehrenbrink and Ravizza,* 2012].

The decline of atmospheric CO_2 has a potential role in initiating glaciation and its increase of terminating it [*Vandenbroucke et al.,* 2010]. Both cases involve changes in silicate weathering rates [*Lenton et al.,* 2012; *Ghienne et al.,* 2014]. The change of $^{187}Os/^{188}Os$ ratios during glacial periods may represent a response to change in silicate weathering, but does not help in tracing the weathering rate or processes involved [*Finlay et al.,* 2010]. The behavior of Li isotopes, however, is solely controlled by silicate weathering processes and, therefore, gives a unique insight into CO_2 drawdown and climate stabilization [*Pogge von Strandmann et al.,* 2017].

Biological processes do not lead to lithium isotope fractionation [*Pogge von Strandmann et al.,* 2017], and carbonate weathering does not affect Li isotope signals [*Dellinger et al*., 2017]. The δ^7Li of primary silicate rocks have a narrow range [*Sauzeat et al.,* 2015] if compared to the high variability of modern rivers which reflects weathering processes, particularly the extent of preferential uptake of ^6Li into secondary minerals [*Dellinger et al*., 2017]. Marine carbonates have a negligible sink of Li [*Marriott et al.,* 2004; *Pogge von Strandmann et al.,* 2013].

A comprehensive review on lithium isotope geochemistry is found in *Tomascak et al*. [2016] and *Penniston-Dorland*

et al. [2017] in which the possibility of use of Li isotope in chemostratigraphy has been overlooked. Lithium isotope chemostratigraphy of Late Ordovician bulk carbonate sections and brachiopods in Anticosti Island, Canada [*Achab et al.,* 2013] (Pointe Laframboise Ellis Bay West), and of an equivalent shale section at Dob's Linn, United Kingdom [*Finlay et al.,* 2010; *Melchin et al.,* 2013], was presented by *Pogge von Strandmann et al*. [2017]. In all sections in that study, the relative timings of δ^7Li and the Hirnantian carbon isotope excursion (HICE) are similar, suggesting that Li isotope excursions occur contemporaneously, consistent with the Li residence time in the ocean (1 Myr). The positive δ^7Li excursion during the Hirnantian cooling event compares well to negative δ^7Li during warming events [*Pogge von Strandmann et al.,* 2013; *Lechler et al.,* 2015].

1.2.10. Elemental Chemostratigraphy

Elemental chemostratigraphy (element and element ratios) is a supplementary, useful tool in stratigraphy, and Mo, Ir, V, Ni, Cu, P, Hg, REEs, and Fe are among the most used elements, while Mo/Al, U/Mo, Rb/K, V/Cr, Zr/Ti, I/Ca, Li/Ca, B/Ca, Sr/Ca, Mg/Ca, Mo/Th, V/Th, and Th/U ratios seem to be particularly interesting. Paleoceanographic applications of trace-metal concentration data have been reviewed by *Algeo and Rowe* [2012].

Iron speciation has been widely used to determine the redox state of ancient basins. The method involves sequential extraction procedures to extract highly reactive iron (oxide, carbonates, and sulfide) and compare their concentration to total iron (Fe_{HR}/Fe_T; *Canfield*, 1989; *Shen et al.,* 2003; *Poulton and Canfield*, 2005). Sediments deposited in an oxygenated water column yield Fe_{HR}/Fe_T lower than 0.38 [*Canfield*, 1989]. Furthermore, the sulfide-bound iron (Fe_P) can be compared to highly reactive iron (Fe_P/Fe_{HR}), with values higher than 0.8 characterizing sulfidic (euxinic) basins [*Canfield et al.,* 2008]. Iron speciation chemostratigraphy has been applied successfully to sedimentary units of different ages, from the Archean to recent [e.g., *Shen et al.,* 2003; *Poulton et al.,* 2004; *Canfield et al.,* 2008; *Lyons et al.,* 2009; *Johnston et al.,* 2010; *Scott et al.,* 2011; *Hammarlund et al.,* 2012; *Frei et al.,* 2013].

In sediments deposited immediately after major glacial events, Hg tends to concentrate as a result from leaching of volcanogenic Hg from land surface and accumulation along argillaceous sediments [*Santos et al.,* 2001]. This element is usually found in low geological background concentrations, and this makes this trace element suitable for identifying accumulation pulses in sediments that can be tentatively related to weathering processes and thus to climatic changes.

Carbon dioxide buildup in the atmosphere during the Neoproterozoic glacial events resulted from volcanism that led to enhanced greenhouse effect, ice melting, and cap carbonate deposition [e.g., *Hoffman et al.,* 1998a; *Hoffman*, 2011]. Besides, intense volcanism may have witnessed the P-T and Cretaceous-Paleogene transition (K-Pg) and was, perhaps, co-responsible for dramatic climatic changes and thus for the decrease in biodiversity and mass extinction [e.g., *Keller*, 2005; *Archibald et al*., 2010]. *Sial et al*. [2010b] demonstrated the use of Hg chemostratigraphy of the cap carbonates to document intense volcanism and resultant CO_2 buildup in the atmosphere, following the Neoproterozoic snowball events. Moreover, Hg chemostratigraphy was applied to investigate the relationships between large igneous province (LIP) activity, abrupt environmental changes, and mass extinctions [e.g., *Nascimento-Silva et al.,* 2011, 2013; *Sanei et al.,* 2012; *Sial et al*., 2013a, 2014, 2016, 2017, this volume; *Adatte et al.,* 2015; *Grasby et al.,* 2013, 2015, 2017; *Percival et al.,* 2015, 2017; *Font et al.,* 2016, 2018; *Thibodeau et al.,* 2016; *Charbonnier et al.,* 2017; *Jones et al.,* 2017; *Thibodeau and Bergquist*, 2017; *Keller et al.,* 2018). To assure that the measured Hg contents result from true Hg loading to the environment, it is necessary to examine Hg/TOC ratios for chemostratigraphy [e.g., *Grasby et al.,* 2015; *Percival et al.,* 2015]. Mercury enrichments in sedimentary successions that recorded the mid-Cenomanian Event and Oceanic Anoxic Event 2 (OAE2) in the Late Cretaceous have been regarded by *Scaife et al*. [2017] as a marker for submarine LIP volcanism, and Hg enrichment recorded in the PETM is assumed to be related to volcanic activity of the North Atlantic Igneous Province (NAIP) (e.g., *Keller et al.,* 2018). Hg is doubtless a good benchmark for high volcanic activity, but normalization by TOC is in some cases problematic if TOC values are <0.2, leading to exaggerated peaks.

Mo and V chemostratigraphy may be useful in the investigation of the redox state of deep ocean water. Mo is a redox-sensitive element, scavenged from seawater into sediments in the form of $MoSxO_{4-}x^{2-}$, under anoxic conditions [*Wen et al.,* 2015]. The transfer of aqueous Mo to the sediment can be increased by means of metal-oxyhydroxide particulate shuttles, but aqueous U is not affected by this process [*Tribovillard et al.,* 2012]. Therefore, an increase in U/Mo ratio may suggest oxic conditions [e.g., *Sosa-Montes et al.,* 2017]. According to *Scheffler et al*. [2003], certain elemental ratios can be useful as proxies for investigation of salinity variation (Rb/K), redox state (V/Cr), or provenance (Zr/Ti). Mo and V can be normalized with Th (Mo/Th and V/Th) and, together with other redox-sensitive trace elements such as Ni, Zn, and Pb, can be used to determine redox variations in ancient sedimentary successions [*Spangenberg et al.,* 2014].

REE has been extensively used in different types of sedimentary rocks, often in combination with yttrium (REEY). The most widely used proxies are Ce, Eu, and Pr

anomalies (Ce/Ce*, Eu/Eu*, Pr/Pr*), Y/Ho, La/Yb, and ΣREE, which can be applied to shales, carbonates, BIF, cherts, phosphorites, and other fine-grained rocks [*Elderfield and Greaves*, 1982; *Liu et al.,* 1988; *Bau and Dulski*, 1996; *Kato et al.,* 2006; *Lawrence and Kamber*, 2006; see *Sial et al.,* 2015b for an overview of proxies]. REE chemostratigraphy has been applied to Archean [*Kamber et al.,* 2014], Paleoproterozoic [*Bau and Dulski*, 1996], Mesoproterozoic [*Azmy et al.,* 2009], Neoproterozoic [*Tribovillard et al*., 2006; *Frimmel*, 2009; *Sansjofre et al.,* 2014; *Spangenberg et al.,* 2014; *Gaucher et al.,* 2015; *Sial et al.,* 2015b; *Hu et al.,* 2016; *Rodler et al.,* 2016], and Phanerozoic successions [*Schmitz et al.,* 1988; *Lécuyer et al.,* 2004; *Fio et al.,* 2010].

The redox behavior of iodine is well known [*Broecker et al.,* 1982]. Besides, it is also known that there is a linear covariation between carbonate-associated iodine (CAI) and IO_3^- during calcite precipitation, but I^- is completely excluded [*Lu et al.,* 2010]. This trait, coupled with the residence time of iodine in seawater (300 ky; *Broecker et al.,* 1982) and concentration near 450 nM in modern ocean, makes I/Ca (or I/Ca + Mg) ratios in carbonates a robust indicator of the presence of IO_3^- and hence oxygen in the water column. Therefore, surface ocean oxygenation has been investigated using I/Ca ratios as a paleoredox indicator [e.g., *Hardisty et al.,* 2014].

Li/Ca and B/Ca in carbonates are regarded as proxies for carbonate saturation state [*Hall and Chan*, 2004; *Hall et al.,* 2005; *Lear and Rosenthal*, 2006; *Yu and Elderfield,* 2007; *Foster*, 2008], and Mg/Ca ratios of foraminiferal shells have been regarded as useful paleothermometer to determine ocean temperature. The difference in the Mg/Ca ratio of the foraminiferal shell and that from a baseline value (defined by the global ocean Mg and Ca concentration) when calibrated for the vital effects of the organism is a function of temperature [e.g., *Lea et al.,* 2000; *Lear et al*., 2000]. The baseline composition of seawater is relatively simple to infer, once both Mg and Ca have long residence times in the oceans (>1 Ma) and are major components of ocean salts.

1.3. CHEMOSTRATIGRAPHY AND CHRONOSTRATIGRAPHIC BOUNDARIES

The International Commission on Stratigraphy (ICS) recognizes the existence of one hundred fourteen chronostratigraphic boundaries. Sixty-seven sections straddling chronostratigraphic boundaries were internationally agreed upon as reference points to define the lower boundaries of stages on the geologic time scale, the Global Boundary Stratotype Section and Point (GSSP), and a golden spike is placed precisely at the boundary defined. Accessibility and degree of representativity of the same boundary on sections worldwide are among the most important criteria in the GSSP selection. Since GSSPs require well-preserved sections of rock without interruptions in sedimentation, and since most are defined by different biozones, defining them becomes more difficult as one goes further back in time in the Precambrian.

So far, chemostratigraphy has been overlooked as a formal criterion on GSSP selection. Carbon isotope excursions (CIE) have been reported only from seven of the established GSSPs [*Cooper et al.,* 2001; *Dupuis et al.,* 2003; *Peng et al.,* 2004; *Knoll et al.,* 2006; *Xu et al.,* 2006; *Aubry et al.,* 2007; *Goldman et al.,* 2007; *Schmitz et al.,* 2011; *Keller et al.,* 2018], probably due to the absence of carbonate rocks in several chronostratigraphic boundary sections. Only in the selection of the Cretaceous-Paleogene (K-Pg; *Molina et al.,* 2006, 2009) and the Paleocene-Eocene (PETM; *Aubry et al.,* 2007) GSSPs was carbon isotope chemostratigraphy one of the criteria, and hydrogen isotopes in the Pleistocene–Holocene GSSP [*Walker et al.,* 2009]. In addition, oxygen isotopes have been reported from two other GSSPs [*Steininger et al.,* 1997; *Hilgen et al.,* 2009]. Heavy element (e.g., Ir, Os, Hg) enrichments at the Cretaceous-Tertiary boundary are well known since the seminal paper of *Alvarez et al*. [1980] and later studies [e.g., *Schmitz et al.,* 1988; *Frei and Frei*, 2002; *Sial et al.,* 2016; *Keller et al.,* 2018, and references therein].

1.4. CHEMOSTRATIGRAPHY AS FORMAL STRATIGRAPHIC METHOD

The stratigraphic record shows changes of the concentration of certain elements with time [*Morante et al.,* 1994], as a function of geological conditions including, but not limited to, tectonic, climatic, redox, oceanographic, biotic, and other processes. Chemostratigraphy enables not only apparently uniform thick successions to be subdivided and correlated with coeval strata located elsewhere [*Ramkumar*, 1999] but also thinner and more heterogeneous sedimentary records. Initially, chemostratigraphy was applied to recognize unique geochemical compositions for characterizing depositional units and correlating them with coeval strata elsewhere and found its use in the stratigraphic location of boundaries and later expanded to examination of specific causes to the stratigraphic variations of geochemical compositions [*Ramkumar et al.,* 2010, 2011]. The utility of chemostratigraphy for age determination was demonstrated through documentation of stratigraphic variations of isotopic trends, beginning with oxygen isotopes. Linear, secular, cyclic, and perturbed trends have been recognized, which are utilized for stratigraphic classification and spatial correlation [e.g., *Zachos et al.,* 2001; *Ramkumar*, 2014, 2015]. In addition, the chemozones, calibrated with absolute time, are in use as chemochrons. Although chemostratigraphy is firmly recognized as a

valid stratigraphic method since more than thirty years [e.g., *Berger and Vincent*, 1981], given to its sensitivity and wide applications, time has come to recognize this technique as an individual method of stratigraphy. The International Stratigraphic Commission (ISC) defines stratigraphy as "the description of all rock bodies forming the Earth's crust and their organization into distinctive, useful, mappable units based on their inherent properties or attributes… in order to establish their distribution and relationship in space and their succession in time, and to interpret geologic history" [*Salvador*, 1994]. Chemostratigraphy "recognizes and organizes" rock bodies into useful units based on their inherent chemical properties. Most importantly, it helps in establishing the distribution and relationships of these units in space and time and, especially, interpreting geological history. In many cases, the resolution of chemostratigraphy proves to be better than other conventional methods of stratigraphy and can be refined by improving sampling resolution, although cyclostratigraphy can be even better, providing a resolution on Milankovitch time scales, reaching back far into the Cenozoic. In this regard, it can be stated that chemostratigraphy as an independent stratigraphic method can serve well even where other methods fail or have limitations. Chemostratigraphy is complementary to other types of stratigraphic units, such as lithostratigraphy, biozones, and magnetostratigraphy. With these attributes in mind, we are of the opinion that chemostratigraphy can be recognized as an independent standard method of stratigraphic classification.

ACKNOWLEDGMENTS

We express our thankfulness to the American Geophysical Union (AGU)/Wiley for the invitation to compile a special publication on "chemostratigraphy across major chronological eras." Three anonymous reviewers are thanked for thorough, critical analysis of the original manuscript. This is the contribution n. 287 from the Nucleus for Geochemical Studies–Stable Isotope Laboratory (NEG-LABISE), Department of Geology, Federal University of Pernambuco, Brazil.

REFERENCES

Achab, A., Asselin, E., Desrochers, A., Riva, J.F., 2013. The end-Ordovician chitinozoan zones of Anticosti Island, Quebec: Definition and stratigraphic position. Review of Palaeobotany and Palynology *198*, 92–109.

Adatte, T., Keller, G., Schoene, B., Samperton, K.M., Font, E., Sial, A.N., Lacerda, L.D., Punekar, J., Fantasia, A., Khadri, S., 2015. Paleoenvironmental influence of Deccan volcanism relative to the KT extinction. Geological Society of America Abstracts with Programs *47*(7), 210, Baltimore.

Ader, A., Sansjofre, P., Halverson, G.P., Busigny, V., Trindade, R.L.F., Kunzmann, M., Nogueira, A.C.R., 2014. Ocean redox structure across the Late Neoproterozoic Oxygenation Event: A nitrogen isotope perspective. Earth and Planetary Science Letters *396*, 1–13.

Algeo, T.J., Rowe, H., 2012. Paleoceanographic applications of trace-metal concentration data. Chemical Geology *324–325*, 6–18.

Algeo, T., Rowe, H., Hower, J.C., Schwark, L., Herrmann, A., Heckel, P., 2008. Changes in ocean denitrification during late carboniferous glacial interglacial cycles. Nature Geoscience *1*, 709–714.

Allen, P.A., Etienne, J.L., 2008. Sedimentary challenge to snowball Earth. Nature Geoscience *1*, 817–825.

Alvarez, L.W., Alvarez, W., Asaro, F., Michel, H.V., 1980. Extraterrestrial cause for the Cretaceous–Tertiary extinction. Science *208*, 1095–1108.

Archibald, J.D., Clemens, W.A., Padian, K., Rowe, T., Macleod, N., Barrett, P.M., Gale, A., Holroyd, P., Sues, H.D., Arens, N.C., Horner, J.R., Wilson, G.P., Goodwin, M.B., Brochu, C.A., Lofgren, D.L., Hurlbert, S.H., Hartman, J.H., Eberth, D.A., Wignall, P.B., Currie, P.J., Weil, A., Prasad, G.V., Dingus, L., Courtillot, V., Milner, A., Milner, A., Bajpai, S., Ward, D.J., Sahni, A., 2010. Cretaceous extinctions: Multiple causes. Science *328*, 973–976.

Arnold, G.L., Anbar, A.D., Barling, J., Lyons, T.W., 2004. Molybdenum isotope evidence for widespread anoxia in mid-Proterozoic oceans. Science *304*, 87–90.

Aubry, M.-P., Ouda, K., Dupuis, C., Berggren, W.A., Van Couvering, J.A., Working Group on the Paleocene/Eocene Boundary, 2007. The Global Standard Stratotype-section and Point (GSSP) for the base of the Eocene Series in the Dababiya section (Egypt). Episodes *30*, 271–286.

Azmy, K., Sylvester, P., de Oliveira, T.F., 2009. Oceanic redox conditions in the Late Mesoproterozoic recorded in the upper Vazante Group carbonates of São Francisco Basin, Brazil: Evidence from stable isotopes and REEs. Precambrian Research *168*(3), 259–270.

Azmy, K., Lavoie, D., Wang, Z., Brand, U., Al-Aasm, I., Jackson, S., Girard, I., 2013. Magnesium isotope and REE composition of Lower Ordovician carbonates from eastern Laurentia: Implications for the origin of dolomites and limestones. Chemical Geology *356*, 64–75.

Bao, H., Lyons, J.R., Zhou, C., 2008. Triple oxygen isotope evidence for elevated CO_2 levels after a Neoproterozoic glaciations. Nature *453*, 504–506.

Bao, H., Fairchild, I.J., Wynn, P.M., Spötl, C., 2009. Stretching the envelope of past surface environments: Neoproterozoic glacial lakes from Svalbard. Science *323*, 119–122.

Baskaran, M., 2012. Handbook of Environmental Isotope Geochemistry. Advances in Isotope Geochemistry. Springer-Verlag, Berlin, 951 pages.

Bau, M., Dulski, P., 1996. Distribution of yttrium and rare-earth elements in the Penge and Kuruman iron-formations, Transvaal Supergroup, South Africa. Precambrian Research *79*(1–2), 37–55.

Beard, B.L., Johnson, C.M., Skulan, J.L., Nealson, K.H., Cox, L., Sun, H., 2003. Application of Fe isotopes to tracing the geochemical and biological cycling of Fe. Chemical Geology *195*, 87–117.

Beaumont, V., Robert, F., 1999. Nitrogen isotope ratios of kerogens in Precambrian cherts: A record of the evolution of atmosphere chemistry? Precambrian Research *96*, 63–82.

Bekker, A., Karhu, J.A., Kaufman, A.J., 2006. Carbon isotope record for the onset of the Lomagundi carbon isotope excursion in the Great Lakes area, North America. Precambrian Research *148*, 145–180.

Berner, R.A., 1990. Atmospheric carbon dioxide levels over Phanerozoic time. Science *249*, 1382–1386.

Berger, W.H., Vincent, E., 1981. Chemostratigraphy and biostratigraphic correlation: Exercises in systemic stratigraphy. Oceanologica Acta *1981*(SP), 115–127.

Berner, E.K., Berner, R.A., 1987. The Global Water Cycle: Geochemistry and Environment. Prentice Hall, New York, 397 p.

Bijl, P.K., Schouten, S., Sluijs, A., Reichart, G.-J., Zachos, J.C., Brinkhuis, H., 2009. Early Palaeogene temperature evolution of the southwest Pacific Ocean. Nature *461*, 776–779.

Blättler, C.L., Henderson, G.M., Jenkys, H.C., 2012. Explaining the Phanerozoic Ca isotope history of seawater. Geology *40*, 843–846.

Bodin, S., Fiet, N, Godet, A., Matera, V., Westermann, S., Clement, A., Janssen, N.M.M., Stille, P, Foellmi, K.B., 2009. Early Cretaceous (late Berriasian to early Aptian) palaeoceanographic change along the northwestern Tethyan margin (Vocontian Trough, southeastern France): $\delta^{13}C$, $\delta^{18}O$ and Sr-isotope and whole-rock records. Cretaceous Research *30*, 1247–1262.

Brenot, A., Cloquet, C., Vigier, N., Carignan, J., France-Lanord, C., 2008. Magnesium isotope systematics of the lithologically varied Moselle river basin, France. Geochimica et Cosmochim Acta *72*, 5070–5089.

Bristow, T.F., Kennedy, M.J., 2008. Carbon isotope excursions and the oxidant budget of the Ediacaran atmosphere and ocean. Geology *36*, 863–866.

Broecker, W.S., Peng, T.H., Beng, Z., 1982. Tracers in the Sea. Lamont-Doherty Geological Observatory, Columbia University, New York, 690 p.

Burke, W.H., Denison, R.E., Hetherington, E.A., Koepnick, R.B.,Nelson, H.F., Otto, J.B., 1982. Variation of seawater $^{87}Sr/^{86}Sr$ throughout Phanerozoic time. Geology *10*, 516–519.

Calver, C.R., Black, L.P., Everard, J.L., Seymour, D.B., 2004. U-Pb zircon age constraints on late Neoproterozoic glaciation in Tasmania. Geology *32*, 892–896.

Canfield, D.E., 1989. Reactive iron in marine sediments. Geochimica et Cosmochimica Acta *53*, 619–632.

Canfield, D.E., 1998. A new model for Proterozoic ocean chemistry. Nature *396*, 450–453

Canfield, D.E., Teske, A., 1996. Late Proterozoic rise in atmospheric oxygen concentration inferred from phylogenetic and sulphur-isotope studies. Nature *381*, 127–132.

Canfield, D.E., Poulton, S.P., Knoll, H., Narbonne, G.M., Ross, G., Goldberg, T., Strauss, H., 2008. Ferruginous conditions dominated later Neoproterozoic deep-water chemistry. Science *321*, 949–952.

Chang, V.T.-C., Masishima, A., Belshaw, N.S., Onions, R.K., 2003. Purification of Mg from low Mg biogenic carbonates for isotope ratio determination using multi-collector ICP-MS. Journal of Analytical Atomic Spectrometry *18*, 296–301.

Charbonnier, G., Morales, C., Duchamp-Alphonse, S., Westermann, S., Adatte, T., Föllmi, K.B., 2017. Mercury enrichment indicates volcanic triggering of Valanginian environmental change. Scientific Reports *7*, 40808, January 2017. doi:10.1038/srep40808.

Chiglino, L., Gaucher, C., Sial, A.N., Bossi, J., Ferreira, V.P., Pimentel, M.M., 2010. Chemostratigraphy of Mesoproterozoic and Neoproterozoic carbonates of the Nico Pérez Terrane, Río de la Plata Craton, Uruguay. Precambrian Research *182*, 313–336.

Claypool, G.E., Holser, W.T., Kaplan, I.R., Sakai, H., Zak, I., 1980. The ages, curves of sulfur and oxygen isotopes in marine sulfate and their mutual interpretation. Chemical Geology *28*, 199–260.

Cooper, R.A., Nowlan, G.S., Williams, S.H., 2001. Global Stratotype Section and Point for base of the Ordovician System. Episodes *24*, 19–28.

Corsetti, F.A., Kaufman, A.J., 2003. Stratigraphic investigations of carbon isotope anomalies and Neoproterozoic ice ages in Death Valley, California. Geological Society of America Bulletin *115*, 916–932.

Cremonese, L., Struck, U., Shields-Zhou, G., Ling, H., Och, L., 2009. $\delta^{15}N$ chemostratigraphy of Ediacaran–Cambrian sections of South China. Supplement Geochimica et Cosmochimica Acta *73*(13S), A-251.

Cremonese, L., Shields-Zhou, G., Struck, U., Ling, H.F., Och, L., Chen, X., Li, D., 2013. Marine biogeochemical cycling during the early Cambrian constrained by a nitrogen and organic carbon isotope study of the Xiaotan section, South China. Precambrian Research *225*, 148–165.

Cremonese, L., Shields-Zhou, G., Struck, U., Ling, H.F., Och, L., 2014. Nitrogen and organic carbon isotope stratigraphy of the Yangtze Platform during the Ediacaran–Cambrian transition in South China. Palaeogeography, Palaeoclimatology, Palaeoecology *398*, 165–186.

Crowe, S.A., Døssing, L.N., Beukes, N.J., Bau, M., Kruger, S.J., Frei, R., Canfield, D.E., 2013. Atmospheric oxygenation three billion years ago. Nature *501*, 535–538.

Dantas, E.L., Alvarenga, C.J.S., Santos, R.V., Pimentel, M.M., 2009. Using Nd isotopes to understand the provenance of sedimentary rocks from a continental margin to a foreland basin in the Neoproterozoic Paraguay Belt, Central Brazil. Precambrian Research *170*, 1–12.

Davies, C.L., Surridge, B.W.J., Gooddy, D.C., 2014. Phosphate oxygen isotopes within aquatic ecosystems: Global data synthesis and future research priorities. Science of the Total Environment *496*, 563–575.

Dellinger, M., Bouchez, J., Gaillardet, J., Faure, L., Moureau, J., 2017. Tracing weathering regimes using the lithium isotope composition of detrital sediments. Geology *45*, 411–414.

DePaolo, D.J., 1988. Neodymium Isotope Geochemistry: An Introduction. Springer-Verlag, Berlin, New York, 187 p.

Dera, G., Puceat, E., Pellenard, P., Neige, P., Delsate, D., Joachimski, M.M., Reisberg, L., Martinez, M., 2009. Water mass exchange and variations in seawater temperature in the NW Tethys during the Early Jurassic; evidence from neodymium and oxygen isotopes of fish teeth and belemnites. Earth and Planetary Science Letters *286*, 198–207.

Døssing, L.N., Dideriksen, K., Stipp, S.L.S., Frei, R., 2011. Reduction of hexavalent chromium by ferrous iron: A process of chromium isotope fractionation and its relevance to natural environments. Chemical Geology *285*, 157–166.

Dupuis, C., Aubry, M.-P., Steurbaut, E., Berggren, W.A., Ouda, K., Magioncalda, R., Cramer, B.S., Kent, D.V., Speijer, R.P., Heilmann-Clausen, C., 2003. The Dababiya Quarry section: Lithostratigraphy, clay mineralogy, geochemistry and paleontology. Micropaleontology *49*, 41–59.

Eagle, R.A., Schauble, E.A., Tripati, A.K., Tutken, T., Hulbert, R.C., Eiler, J.M., 2010. Body temperatures of modern and extinct vertebrates from ^{13}C–^{18}O bond abundances in bioapetite. Proceedings of the National Academy of Sciences *107*, 10377–10382.

Eiler, J.M., 2007. "Clumped-isotope" geochemistry: The study of naturally-occurring, multiply-substituted isotopologues. Earth and Planetary Science Letters *262*, 309–327. doi:10.1016/j.epsl.2007.08.020.

Elderfield, H., Greaves, M.J., 1982. The rare earth elements in seawater. Nature *296*, 214–219.

Emiliani, C. 1955. Pleistocene temperatures. The Journal of Geology *63*(6), 538–578.

Falkowski, P., 2003. Biogeochemistry of primary production in the sea. Treatise on Geochemistry *8*, 185–213.

Fantle, M.S., Tipper, E.T., 2014. Calcium isotopes in the global biogeochemical Ca cycle: Implications for development of a Ca isotope proxy. Earth-Science Review *129*, 148–177.

Farquhar, J., Bao, H., Thiemens, M., 2000. Atmospheric influence of Earth's earliest sulfur cycle. Science *289*, 756–758.

Finlay, A.J., Selby, D., Grocke, D.R., 2010. Tracking the Hirnantian glaciation using Os isotopes. Earth and Planetary Science Letters *293*, 339–348.

Fio, K., Spangenberg, J.E., Vlahović, I., Sremac, J., Velić, I., Mrinjek, E., 2010. Stable isotope and trace element stratigraphy across the Permian–Triassic transition: A redefinition of the boundary in the Velebit Mountain, Croatia. Chemical Geology *278*(1), 38–57.

Flament, N., Coltice, N., Rey, P.F., 2011. The evolution of $^{87}Sr/^{86}Sr$ of marine carbonates does not constrain continental growth. Precambrian Research *229*, 177–188. doi:10.1016/j.precamres.2011.10.009.

Font, F., Adatte, T., Sial, A.N., Lacerda, L.D., Keller, G., Punekar, J., 2016. Mercury anomaly, Deccan Volcanism and the end-Cretaceous Mass Extinction. Geology *44*, 171–174. doi:10.1130/G37451.1.

Font, E., Adatte, T., Andrade, M., Keller, G., Mbabi Bitchong, A., Carvallo, C., Ferreira, J., Diogo, Z., Mirão, J., 2018. Deccan volcanism induced high-stress environment during the Cretaceous–Paleogene transition at Zumaia, Spain: Evidence from magnetic, mineralogical and biostratigraphic records. Earth and Planetary Science Letters *484*, 53–66.

Foster, G.L., 2008. Seawater pH, pCO_2 and $[CO_3\ 2-]$ variations in the Caribbean Sea over the last 130 kyr: A boron isotope and B/Ca study of planktic foraminifera. Earth Planetary Science Letters *271*, 254–66.

Foster, G.L., Rae, J.W.B., 2016. Reconstructing ocean pH with boron isotopes in foraminifera. Annual Reviews Earth Planetary Science *44*, 207–37.

Foster, G.L., Pogge von Strandmann, P.A.E., Rae, J.W.B., 2010 Boron and magnesium isotopic composition of seawater. Geochemistry, Geophysics, Geosystems *11*, 1–10.

Frei, R., Frei, K.M., 2002. A multi-isotopic and trace element investigation of the Cretaceous–Tertiary boundary layer at Stevns Klint, Denmark–inferences for the origin and nature of siderophile and lithophile element geochemical anomalies. Earth and Planetary Science Letters *203*(2), 691–708.

Frei, R., Gaucher, C., Poulton, S.W., Canfield, D.E., 2009. Fluctuations in Precambrian atmospheric oxygenation recorded by chromium isotopes. Nature *46*, 250–254.

Frei, R., Gaucher, C., Døssing, L.N., Sial, A.N., 2011. Chromium isotopes in carbonates: A tracer for climate change and for reconstructing the redox state of ancient seawater. Earth Planetary Sciences Letters *312*, 114–125.

Frei, R., Gaucher, C., Stolper, D., Canfield, D.E., 2013. Fluctuations in late Neoproterozoic atmospheric oxidation: Cr isotope chemostratigraphy and iron speciation of the late Ediacaran lower Arroyo del Soldado Group (Uruguay). Gondwana Research *23*, 797–811.

Frei, R., Døssing, L.N., Gaucher, C., Boggiani, P.C., Frei, K.M., Bech Árting, T., Crowe, S.A., Freitas, B.T., 2017. Extensive oxidative weathering in the aftermath of a late Neoproterozoic glaciation: Evidence from trace element and chromium isotope records in the Urucum district (Jacadigo Group) and Puga iron formations (Mato Grosso do Sul, Brazil). Gondwana Research *49*, 1–20.

Friedrich, O., Norris, R.D., Erbacher, J., 2012. Evolution of middle to Late Cretaceous oceans: A 55 m.y. record of Earth's temperature and carbon cycle. Geology *40*, 107–110.

Frimmel, H.E., 2008. REE geochemistry of Neoproterozoic carbonates: Deviations from normal marine signatures. *Abstract, 33 International Geological Congress*, Oslo, Norway.

Frimmel, H.E., 2009. Trace element distribution in Neoproterozoic carbonates as palaeoenvironmental indicator. Chemical Geology *258*, 338–353.

Frimmel, H.E., 2010. On the reliability of stable carbon isotopes for Neoproterozoic chemostratigraphic correlation. Precambrian Research *182*, 239–252.

Frost, C.D., von Blanckenburg, F., Schoenberg, R., Frost, B.R., Swapp, S.M., 2007. Preservation of Fe isotope heterogeneities during diagenesis and metamorphism of banded iron formation. Contributions Mineralogy Petrology *153*, 211–235.

Galy, A., Bar-Matthews, M., Halicz, L., O'Nions, R.K., 2002. Mg isotopic composition of carbonate: Insight from speleothem formation. Earth Planetary Science Letters *201*, 105–115.

Gaucher, C., Sial, A.N., Ferreira, V.P., Pimentel, M.M., Chiglino, L., Sprechmann, P., 2007. Chemostratigraphy of the Cerro Victoria Formation (Lower Cambrian, Uruguay): Evidence for progressive climate stabilization across the Precambrian–Cambrian boundary. Chemical Geology *237*, 28–46.

Gaucher, C., Sial, A.N., Frei, R., 2015. Chemostratigraphy of Neoproterozoic banded iron formation (BIF): Types, age and origin. In: Ramkumar, M. (Ed.), Chemostratigraphy: Concepts Techniques and Applications. Elsevier, Amsterdam, pp. 433–449.

Geske, A., Goldstein, R.H., Mavromatis, V., Richter, D.K., Buhl, D., Kluge, T., John, C.M., Immenhauser, A., 2015. The magnesium isotope ($\delta^{26}Mg$) signature of dolomites. Geochimica et Cosmochimica Acta *149*, 131–151.

Ghienne, J.-F., Desrochers, A., Vandenbroucke, T.R.A., Achab, A., Asselin, E., Dabard, M.-P., Farley, C., Loi, A., Paris, F., Wickson, S., Veizer, J., 2014. A Cenozoic-style scenario for the end-Ordovician glaciation. Nature Communications *5*, 4485. doi:10.1038/ncomms5485.

Ghosh, P., Adkins, J., Affek, H., Balta, B., Guo, W., Schauble, E.A., Schrag, D., Eiler, J.M., 2006. ^{13}C-^{18}O bonds in carbonate minerals: A new kind of paleothermometer. Geochimica et Cosmochimica Acta *70*, 1439–1456.

Goldman, D., Leslie, S.A., Nõlvak, J., Young, S., Bergström, S.M., Huff, W.D., 2007. The Global Stratotype Section and Point (GSSP) for the base of the Katian Stage of the Upper Ordovician Series at Black Knob Ridge, Southeastern Oklahoma, USA. Episodes *30*, 258–270.

Grasby, S.E., Sanei, H., Beauchamp, B., Chen, Z., 2013. Mercury deposition through the Permo–Triassic Biotic Crisis. Chemical Geology *351*, 209–16.

Grasby, S.E., Beauchamp, B., Bond, D.P.G., Wignall, P.B., Sanei, H., 2015. Mercury anomalies associated with three extinction events (Capitanian Crisis, Latest Permian Extinction and the Smithian/Spathian Extinction) in NW Pangea. Geological Magazine *153*, 285–297.

Grasby, S.E., Shen, W., Yin, R., Gleason, J.D., Blum, J.D., Lepak, R.F., Hurley, J.P., Beauchamp, B., 2017. Isotopic signatures of mercury contamination in latest Permian oceans. Geology *45*, 55–58.

Grotzinger, J.P., Fike, D.A., Fischer, W.W., 2011. Enigmatic origin of the largest-known carbon isotope excursion in Earth's history. Nature Geoscience *4*, 285–291.

Guo, Q., Strauss, H., Kaufman, A.J., Schröder, S., Gutzmer, J., Wing, B., Baker, M.A., Bekker, A., Jin, Q., Kim, S.-T., Farquhar, J., 2009a. Reconstructing Earth's surface oxidation across the Archean–Proterozoic transition. Geology *3*, 399–402.

Guo, W., Mosenfelder, J.L., Goddard, W.A., III, Eiler, J.M., 2009b. Isotopic fractionations associated with phosphoric acid digestion of carbonate minerals: Insights from first-principles theoretical modeling and clumped isotope measurements. Geochimica et Cosmochimica Acta *73*, 7203–7225.

Gussone, N., Schmitt, A.-D., Heuser, A., Wmbacher, F., Dietzel, M., Tipper, E., Schiller, M., 2016. Calcium Isotope Geochemistry. Advances in Isotope Geochemistry. Springer, Berlin, Heidelberg, 260 p. doi:10.1007/978-3-540-68953-9.

Halevy, I., Johnston, D., Schrag, D., 2010. Explaining the structure of the Archean mass-independent sulfur isotope record. Science *329*, 204–207

Hall, J.M., Chan, L.H., 2004. Li/Ca in multiple species of benthic and planktonic foraminifera: Thermocline, latitudinal, and glacial–interglacial variation. Geochimica Cosmochimica Acta *68*, 529–545.

Hall, J.M., Chanb, T.L.-H., McDonough, W.F., Turekian, K.K., 2005. Determination of the lithium isotopic composition of planktic foraminifera and its application as a paleo-seawater proxy. Marine Geology *217*, 255–265.

Halverson, G.P., Hoffman, P.F., Schrag, D.P., Maloof, A.C., Hugh, A., Rice, N., 2005. Towards a Neoproterozoic composite carbon-isotope record. Geological Society of America Bulletin *117*, 1181–1207.

Halverson, G.P., Dudás, F.Ö., Maloof, A., Bowring, S.A., 2007. Evolution of the $^{87}Sr/^{86}Sr$ composition of Neoproterozoic seawater. Palaeogeography, Palaeoclimatology, Palaeoecology *256*, 103–129.

Halverson, G.P., Hurtgen, M.T., Porter, S.M., Collins, A.S., 2010a. Neoproterozoic–Cambrian biogeochemical evolution. In: Gaucher, C., Sial, A.N., Halverson, G.P., Frimmel, H. (Eds.), Neoproterozoic-Cambrian Tectonics, Global Change and Evolution: A Focus on South Western Gondwana. Developments in Precambrian Geology *16*. Elsevier, Amsterdam, Boston, pp. 351–365.

Halverson, G.P., Wade, B.P., Hurtgen, M.T., Barovich, K., 2010b. Neoproterozoic chemostratigraphy. In: Karhu, J., Sial, A.N., Ferreira, V.P. (Eds.), Precambrian Isotope Stratigraphy, special issue. Precambrian Research *182*. Elsevier, Amsterdam, pp. 337–350.

Halverson, G.P., Poitrasson, F., Hoffman, P.F., Nedelec, A., Montel, J.M., Kirby, J., 2011. Fe isotope and trace element geochemistry of the Neoproterozoic syn-glacial Rapitan iron formation. Earth Planetary Science Letters *309*, 100–112.

Hammarlund, E.U., Dahl, T.W., Harper, D.A., Bond, D.P., Nielsen, A.T., Bjerrum, C.J., Schovsbo, N.H., Schönlaub, H.P., Zalasiewicz, J.A., Canfield, D.E., 2012. A sulfidic driver for the end-Ordovician mass extinction. Earth and Planetary Science Letters *331*, 128–139.

Hardisty, D.S., Lu, Z., Planavsky, N.J., Bekker, A., Philippot, P., Zhou, Z., Lyons, T.W., 2014. An iodine record of Paleoproterozoic surface ocean oxygenation. Geology *42*, 619–622.

Heimann, A., Johnson, C.M., Beard, B.L., Valley, J.W., Roden, E.E., Spicuzza, M.J., Beukes, N.J., 2010. Fe, C, and O isotope compositions of banded iron formation carbonates demonstrate a major role for dissimilatory iron reduction in 2.5 Ga marine environments. Earth Planetary Science Letters *294*, 8–18.

Hemming, N.G., Hönisch, B., 2007. Boron isotopes in marine carbonate sediments and the pH of the Ocean. Developments in Marine Geology *1*, 717–734.

Herrle, J.O., Pross, J., Friedrich, O., Koßler, P., Hemleben, C., 2003. Forcing mechanisms for mid-Cretaceous black shale formation: Evidence from the Upper Aptian and Lower Albian of the Vocontian Basin (SE France). Palaeogeography, Palaeoclimatology, Palaeoecology *190*, 399–426.

Higgins, J.A., Schrag, D.P., 2010. Constraining magnesium cycling in marine sediments using magnesium isotopes. Geochimica Cosmochimica Acta *74*, 5039–5053.

Hilgen, F.J., Abels, H.A., Iaccarino, S., Krijgsman, H., Raffi, I., Sprovieri, R., Turco, E., Zachariasse, E.W., 2009. The Global Stratotype Section and Point (GSSP) of the Serravallian Stage (Middle Miocene). Episodes *32*, 152–166.

Hoffman, P.F., 2011. Strange bedfellows: Glacial diamictite and cap carbonate from the Marinoan (635 Ma) glaciation in Namibia. Sedimentology *58*, 57–119.

Hoffman, P.F., Kaufman, A.J., Halverson, G.P., Schrag, D.P., 1998a. A Neoproterozoic snowball Earth. Science *281*, 1342–1346.

Hoffman, P.F., Kaufman, A.J., Halverson, G.P., 1998b. Comings and goings of global glaciations on a Neoproterozoic tropical platform in Namibia. GSA Today *8*, 1–9.

Holser, W.T., 1997. Geochemical events documented in inorganic carbon isotopes. Palaeogeography, Palaeoclimatology, Palaeoecology *132*, 173–182.

Hönisch, B., Ridgwell, A., Schmidt, D.N., Thomas, E., Gibbs, S.J., Sluijs, A., Zeebe, R., Kump, L., Martindale, R.C., Greene, S.E., Kiessling, W., Ries, J., Zachos, J.C., Royer, D.L., Barker, S., Marchitto, T.M., Jr., Moyer, R., Pelejero, C., Ziveri, P., Foster, G.L., Williams, B., 2012. The geological record of ocean acidification. Science *335*, 1058. doi:10.1126/science.1208277.

Hu, R., Wang, W., Li, S.-K.,Yang, Y.-Z., Chen, F., 2016. Sedimentary environment of Ediacaran sequences of South China: Trace element and Sr-Nd isotope constraints. The Journal of Geology *124*, 769–789.

Huang, K.-J., Teng, F.-Z., Shen, B., Xiao, S., Lang, X., Ma, H.-R., Fu, Y., Peng, Y., 2016. Episode of intense chemical weathering during the termination of the 635 Ma Marinoan glaciation. Proceedings of the National Academy of Science *113*, 14904–14909.

Jacobsen, S.B., Kaufman, A.J., 1999. The Sr, C and O isotopic evolution of Neoproterozoic seawater. Chemical Geology *161*, 37–57.

Jarvis, I., Lignum, J.S., Gröcke, D.R., Jenkyns, H.C., Pearce, M.A., 2011. Black shale deposition, atmospheric CO_2 drawdown, and cooling during the Cenomanian-Turonian Oceanic Anoxic Event. Paleoceanography *26*, PA3201. doi:10.1029/2010PA002081.

Jenkyns, H.C., 2003. Evidence for rapid climate change in the Mesozoic–Palaeogene greenhouse world. Philosophical Transactions of the Royal Society of London *361*, 1885–1916.

Jenkyns, H.C., 2010. Geochemistry of oceanic anoxic events. Geochemistry, Geophysics, Geosystems *11*(3). doi:10.1029/2009GC002788.

Jenkyns, H.C., Clayton, C.J., 1986, Black shales and carbon isotopes from the Tethyan Lower Jurassic. Sedimentology *33*, 87–106.

Jenkyns, H.C., Gröcke, D.R., Hesselbo, S.P., 2001. Nitrogen isotope evidence for water mass denitrification during the early Toarcian (Jurassic) oceanic anoxic event. Paleoceanography *16*(6), 593–603. doi:10.1029/2000PA000558.

Jenkyns, H.C., Matthews, A., Tsikos, H., Erel, Y., 2007. Nitrate reduction, sulfate reduction, and sedimentary iron isotope evolution during the Cenomanian–Turonian oceanic anoxic event. Paleoceanography *22*, PA3208. doi:10.1029/2006PA001355.

Jenkyns, H., Schouten-Huibers, L., Schouten S., Sinninghe-Damste, J.S., 2012. Warm Middle Jurassic-early Cretaceous high-latitude sea surface temperature from the Southern Ocean. Climate of the Past *8*, 215–226.

Joachimski, M.M., Buggisch, W. 2002. Conodont apatite $\delta^{18}O$ signatures indicate climatic cooling as a trigger of the Late Devonian mass extinction. Geology *30*, 711–714.

Joachimski, M.M., Simon, L., Van Geldern, R., Lécuyer, C., 2005. Boron isotope geochemistry of Paleozoic brachiopod calcite: Implications for a secular change in the boron isotope geochemistry of seawater over the Phanerozoic. Geochimica et Cosmochimica Acta *69*, 4035–4044.

Johnson, C., Beard, L., 2006. Fe isotopes: An emerging technique for understanding modern and ancient biogeochemical cycles. GSA Today *16*, 4–10.

Johnson, C.M., Beard, B.L., Beukes, N.J., Klein, C., O'Leary, J.M., 2003. Ancient geochemical cycling in the Earth as inferred from Fe isotope studies of banded iron formations from the Transvaal Craton. Contributions to Mineralogy and Petrology *114*, 523–547.

Johnson, C.M., Beard, B.L., Albarede, F., 2004. Geochemistry of non-traditional stable isotopes. Reviews in Mineralogy and Geochemistry *55*, 454 pp.

Johnson, C.M., Beard, B.L., Roden, E.E., 2008. The iron isotope fingerprints of redox and biogeochemical cycling in modern and ancient oceans. Annual Reviews Earth Planetary Science *36*, 457–493.

Johnston, D.T., Poulton, S.W., Dehler, C., Porter, S., Husson, J., Canfield, D.E., Knoll, A.H., 2010. An emerging picture of Neoproterozoic ocean chemistry: Insights from the Chuar Group, Grand Canyon, USA. Earth and Planetary Science Letters *290*, 64–73.

Jones, C.E., Jenkyns, H.C., 2001. Seawater strontium isotopes, oceanic anoxic events, and seafloor hydrothermal activity in the Jurassic and Cretaceous. American Journal of Science *301*, 112–149.

Jones, D.S., Martini, A.M., Fike, A., Kaiho, K., 2017. A volcanic trigger for the Late Ordovician mass extinction? Mercury data from south China and Laurentia. Geology *45*(7), 631–634. doi:10.1130/G38940.1.

Kah, L.C., Sherman, A.G., Narbonne, G.M., Knoll, A.H., Kaufman, A.J., 1999. $\delta^{13}C$ stratigraphy of the Proterozoic by lot supergroup, Baffin Islands, Canada: Implications for regional lithostratigraphy correlations. Canadian Journal of Earth Sciences *36*, 313–332.

Kamber, B.S., Webb, G.E., Gallagher, M., 2014. The rare earth element signal in Archaean microbial carbonate: Information on ocean redox and biogenicity. Journal of the Geological Society *171*(6), 745–763.

Karhu, J.A., Holland, H.D., 1996. Carbon isotopes and the rise of atmospheric oxygen. Geology *24*, 867–870.

Karhu, J., Sial, A.N., Ferreira, V.P., 2010. Insights from precambrian isotope stratigraphy. Precambrian Research *182*, 239–412.

Kasemann, S.A., Hawkesworth, C.J., Prave, A.R., Fallick, A.E., Pearson, P.N., 2005. Boron and calcium isotope composition in Neoproterozoic carbonate rocks from Namibia: Evidence for extreme environmental change. Earth Planetary Sciences Letters *23*, 73–86.

Kato, Y., Yamaguchi, K.E., Ohmoto, H., 2006. Rare earth elements in Precambrian banded iron formations: Secular changes of Ce and Eu anomalies and evolution of atmospheric oxygen. Geological Society of America Memoirs *198*, 269–289.

Kaufman, A.J., Knoll, A.H., Awramik, S.M., 1992. Biostratigraphic and chemostratigraphic correlation of Neoproterozoic sedimentary successions: Upper Tindir Group, northwestern Canada, as a test case. Geology *20*, 181–185.

Kaufman, A.J., Jacobsen, S.B., Knoll, A.H., 1993. The Vendian record of C- and Sr-isotopic variations: Implications for tectonics and paleoclimate. Earth and Planetary Science Letters *120*, 409–430.

Kaufman, A.J., Knoll, A.H., Narbonne, G.M., 1997. Isotopes, ice ages, and terminal Proterozoic Earth history. Proceedings of the National Academy Science *94*, 6600–6605.

Kaufman, A.J., Sial, A.N., Ferreira, V.P., (guest editors), 2007a.Precambrian isotope chemostratigraphy. Chemical Geology *237*(1/2), special Issue, 232 p.

Kaufman, A.J., Sial, A.N., Ferreira, V.P., 2007b. Preface to special issue of chemical geology on precambrian chemostratigraphy in honor of the late William T. Holser. Chemical Geology *237*, 1–4.

Kaufman, A.J., Sial, A.N., Frimmel, H.E., Misi, A., 2009. Neoproterozoic to Cambrian Palaeoclimatic events in Southwestern Gondwana. In: Gaucher, C., Sial, A.N., Halverson, G.P., Frimmel, H. (Eds.), Neoproterozoic–Cambrian Tectonics, Global Change and Evolution: A Focus on Southwestern Gondwana. Developments in Precambrian Geology *16*. Elsevier, Amsterdam, pp. 369–388.

Keller, G., 2005. Impacts, volcanism and mass extinction: Random coincidence or cause and effect? Australian Journal of Earth Science *52*, 725–757.

Keller, G., Mateo, P., Punekar, J., Khozyem, H., Gertsch, B., Spangenberg, J., Bitchong, A.M., Adatte, A., 2018. Environmental changes during the Cretaceous–Paleogene mass extinction and Paleocene–Eocene Thermal Maximum: Implications for the Anthropocene. Gondwana Research *56*, 69–89.

Kennedy, M.J., Runnegar, B., Prave, A.R., Hoffmann, K.H., Arthur, M.A., 1998.Two or four Neoproterozoic glaciations? Geology *26*, 1059–1063.

Keto, L.S., Jacobsen, S.B., 1988. Nd isotopic variations of early Paleozoic oceans. Earth Planetary Science Letters *84*, 27–41.

Kikumoto, R., Tahata, M., Nishizawa, M., Sawaki, Y., Maruyama, S., Shu, D., Han, J., Komiya, T., Takai, K., Ueno, Y., 2014. Nitrogen isotope chemostratigraphy of the Ediacaran and Early Cambrian platform sequence at Three Gorges, South China. Gondwana Research *25*(3), 1057–1069.

Klein, C., Beukes, N.J., 1993. Sedimentology and geochemistry of the glaciogenic Late Proterozoic Rapitan Iron Formation in Canada. Economic Geology *88*, 542–565.

Knauth, L.P., Kennedy, M.J., 2009. The late Precambrian greening of the Earth. Nature *460*, 728–732.

Knoll, A.H., Walter, M.R., 1992. Latest Proterozoic stratigraphy and Earth history. Nature *356*, 673–678.

Knoll, A.H., Hayes, J.M., Kaufman, A.J., Swett, K., Lambert, I.B., 1986. Secular variation in carbon isotope ratios from Upper Proterozoic successions of Svalbard and East Greenland. Nature *321*, 832–838.

Knoll, A., Walter, M., Narbonne, G., Christie-Blick, N., 2006. The Ediacaran Period: A new addition to the geologic time scale. Lethaia *39*, 13–30.

Korte, C., Kozur, H.W, 2010. Carbon-isotope stratigraphy across the Permian–Triassic boundary: A review. Journal of Asian Earth Sciences *39*, 215–235.

Kump, L.R., Arthur, M.A., 1999. Interpreting carbon-isotope excursions: Carbonates and organic matter. Chemical Geology *161*, 181–198.

Kuznetsov, A., Melezhik, V., Gorokhov, I., Melnikov, N., Konstantinova, G., Kutyavin, E., Turchenko, T. 2010. Sr isotopic composition of Paleoproterozoic ^{13}C-rich carbonate rocks: The Tulomozero Formation, SE Fennoscandian Shield. Precambrian Research *182*, 300–312.

Lawrence, M.G., Kamber, B.S., 2006. The behaviour of the rare earth elements during estuarine mixing: Revisited. Marine Chemistry *100*(1), 147–161.

Lea, D.W., Pak, D.K., Spero, H.J., 2000. Climate impact of late Quaternary equatorial Pacific sea surface temperature variations. Science *289*, 1719–1724.

Lear, C.H., Y. Rosenthal, 2006. Benthic foraminiferal Li/Ca: Insights into Cenozoic seawater carbonate saturation state, Geology *34*, 985–988. doi:10.1130/G22792A.1.

Lear, C.H., Elderfield, H., Wilson, P.A., 2000. Cenozoic deep-sea temperatures and global ice volumes from Mg/Ca in benthic foraminiferal calcite. Science *287*, 269–272.

Lechler, M., Pogge von Strandmann, P.A.E., Jenkyns, H.C., Prosser, G., Parente, M., 2015. Lithium-isotope evidence for enhanced silicate weathering during OAE 1a (Early Aptian Selli event). Earth and Planetary Science Letters *432*, 210–222.

Leckie, R.M., Bralower, T.J., Cashman, R., 2002, Oceanic anoxic events and plankton evolution: Biotic response to tectonic forcing during the mid-Cretaceous. Paleoceanography *17*, 1041. doi:10.1029/2001PA000623.

Lécuyer, C., Brouxel, M., Albarède, F., 1990 Elemental fluxes during hydrothermal alteration of the Trinity ophiolite (California, USA) by seawater. Chemical Geology *89*, 87–115.

Lécuyer, C., Reynard, B., Grandjean, P., 2004. Rare earth element evolution of Phanerozoic seawater recorded in biogenic apatites. Chemical Geology *204*(1), 63–102.

Lenton, T.M., Crouch, M., Johson, M., Pires, N., Dolan, L., 2012. First plants cooled the Ordovician. Nature Geoscience *5*, 86–89.

Li, W., Chakraborty, S., Beard, B.L., Romanek, C.S., Johnson, C.M., 2012. Magnesium isotope fractionation during precipitation of inorganic calcite under laboratory conditions. Earth Planetary Science Letters *333–334*, 304–316.

Lindsay, J.F., Brasier, M.D., 2002. Did global tectonics drive early biosphere evolution? Carbon isotope record from 2.6 to1.9 Ga carbonates of Western Australian basins. Precambrian Research *114*, 1–34.

Lisiecki, L.E., Raymo, M.E., 2005. A Pliocene-Pleistocene stack of 57 globally distributed benthic δ18O records. Paleoceanography *20*(1), PA1003.

Liu, Y.G., Miah, M.R.U., Schmitt, R.A., 1988. Cerium: A chemical tracer for paleo-oceanic redox conditions. Geochimica et Cosmochimica Acta *52*(6), 1361–1371.

Lu, Z., Jenkyns, H.C., Rickaby, R.E.M., 2010. Iodine to calcium ratios in marine carbonates as a paleo-redox proxy during oceanic anoxic events. Geology *38*, 1107–1110.

Luo, G., Algeo, T.J., Zhan, R., Yan, D., Huang, J., Liu, J., Xie, S., 2016. Perturbation of the marine nitrogen cycle during the Late Ordovician glaciation and mass extinction. Palaeogeography, Palaeoclimatology, Palaeoecology *448*, 339–348.

Lyons, T.W., Reinhard, C.T., 2009. Oxygen for heavy-metal fans. Nature *461*,179–181.

Lyons, T.W., Anbar, A.D., Severmann, S., Scott, C., Gill, B.C., 2009. Tracking euxinia in the ancient ocean: A multiproxy perspective and Proterozoic case study. Annual Review of Earth and Planetary Sciences *37*, 507–534.

Macdougall, J.D., 1991. Radiogenic isotopes in seawater and sedimentary systems In: Heaman, L., Ludden, J.N. (Eds.), Applications of Radiogenic Isotope Systems to Problems in Geology. NMCA Short Course Handbook. Mineralogical Association of Canada, Toronto, ON, pp. 337–364, (Chapter10).

Magaritz, M., 1989. $\delta^{13}C$ minima follow extinction events: A clue to faunal radiation. Geology *17*, 337–340.

Magaritz, M., Holser, W.T., Kirschvink, J.L., 1986. Carbon-isotope events across the Precambrian/Cambrian boundary on the Siberian Platform. Nature *320*, 258–259.

Maloof, A.C., Porter, S.M., Moore, J.H., Dudás, F.O., Bowring, S.A., Higgins, J.A., Fike, D.A., Eddy, M.P., 2010. The earliest Cambrian record of animals and ocean geochemical change. Geological Society of America Bulletin *122*, 1731–1774.

Marriott, C.S., Henderson, G.M., Crompton, R., Staubwasser, M., Shaw, S., 2004. Effect of mineralogy, salinity, and temperature on Li/Ca and Li isotope composition of calcium carbonate. Chemical Geology *212*, 5–15.

Marshall, J.D., 1992. Climatic and oceanographic isotopic signals from the carbonate rock record and their preservation. Geological Magazine *129*, 143–160.

McArthur, J.M., 2010. Strontium isotope stratigraphy. In: Ratcliffe K.T., Zaitlin B.A. (Eds.), Application of Modern Stratigraphic Techniques: Theory and Case Histories. SEPM Special Publication *94*. SEPM (Society for Sedimentary Geology), Tulsa, OK, pp. 129–142.

McArthur, J.M., Howarth, R.J., Bailey, T.R., 2001. Strontium isotope stratigraphy: Lowess version 3: Best fit to the marine Sr-isotope curve for 0–509 Ma and accompanying look-up table for deriving numerical age. Journal of Geology *109*, 155–170.

Melchin, M.J., Mitchell, C.E., Holmden, C., Storch, P., 2013. Environmental changes in the Late Ordovician-early Silurian: Review and new insights from black shales and nitrogen isotopes. Geological Society of America Bulletin *125*, 1635–1670.

Melezhik, V.A., Fallick, A.E., Medvedev, P.V., Marakarikhin, V.V., 1999. Extreme ^{13}Ccarb enrichment in ca. 2.0Ga magnesite–stromatolite–dolomite-'redbeds' association in a global context: A case for the world-wide signal enhanced by a local environment. Earth Science Review *48*, 71–120.

Melezhik, V.A., Gorokov, I.M., Kuznetsov, A.B., Fallick, A.E., 2001. Chemostratigraphy of Neoproterozoic carbonates: Implications for "blind dating". Terra Nova *13*, 1–11.

Melezhik, V.A., Roberts, D., Fallick, A.E., Gorokhov, I.M., Kusnetzov, A.B., 2005. Geochemical preservation potential of high-grade calcite marble versus dolomite marble: Implication for isotope chemostratigraphy. Chemical Geology *216*, 203–224.

Melezhik, V.A., Huhma, H., Fallick, A.E., Whitehouse, M.J., 2007.Temporal constraints on the Palaeoproterozoic Lomagundi-Jatuli carbon isotope event. Geology *35*, 655–658.

Meyer, K.M., Yu, M., Lehrmann, D., van de Schootbrugge, B., Payne, J.L., 2013. Constraints on early Triassic carbon cycle dynamics from paired organic and inorganic carbon isotope records. Earth Planetary Science Letters *361*, 429–435.

Molina, E., Alegret, L., Arenillas, I., Arz, J.A., Gallala, N., Hardenbol, J., Von Salis, K., Steurbaut, E., Vandenberghe, N., Zaghbib-Turki, D., 2006. The global boundary Section and Point for the base of the Danian Stage (Paleocene, Paleogene, "Tertiary", Cenozoic) at El Kef, Tunisia: Original definition and revision. Episodes *29*, 263–273.

Molina, E., Alegret, L., Arenillas, E., Arz, J.A., Gallala, N., Grajales-Nishimura, J.M., Murillo-Muñetón, G., Zaghbib-Turki, D., 2009. The Global Boundary Stratotype Section and Point for the base of the Danian Stage (Paleocene, Paleogene, "Tertiary", Cenozoic): Auxiliary sections and correlation. Episodes *32*, 84–95.

Montañez, I.P., Osleger, D.A., Banner, J., Mack, L.E., Musgrove, M., 2000. Evolution of the Sr and C isotope composition of Cambrian Oceans. GSA Today *10*, 1–7.

Morante, R., Veevers, J.J., Andrew, A.S., Hamilton, P.J., 1994. Determination of the Permian–Triassic boundary in Australia. APEA Journal *34*, 330–336.

Nascimento, R.S.C., Sial, A.N., Pimentel, M.M., 2007. C-and Sr-isotope systematics applied to Neoproterozoic marbles of the Seridó Belt, northeastern Brazil. Chemical Geology *237*, 209–228.

Nascimento-Silva, V.M., Sial, A.N., Ferreira, V.P., Neumann, V.H., Barbosa, J.A., Pimentel, M.M., Lacerda, L.D., 2011. Cretaceous–Paleogene transition at the Paraíba Basin, Northeastern, Brazil: Carbon-isotope and mercury subsurface stratigraphies. Journal of South American Earth Sciences *32*, 379–392.

Nascimento-Silva, M.V., Sial, A.N., Ferreira, V.P., Barbosa, J.A., Neumann, V.H., Pimentel, M.M., Lacerda, L.D., 2013. Carbon Isotopes, rare-earth elements and mercury behavior of Maastrichtian–Danian carbonate succession of the Paraíba Basin, Northeastern Brazil. In: Bojar, A.V., Melinte-Dobrinescu, M.C., Smit, J. (Eds.), Isotopic Studies in Cretaceous Research. Geological Society, London, Special Publications *382*. Geological Society of London, London, pp. 85–104.

Nielsen, S.G., Rehkämper, M., 2012. Thallium isotopes and their application to problems in Earth and environmental science. In: Baskaran, M. (Ed.), Handbook of Environmental Isotope Geochemistry. Advances in Isotope Geochemistry. Springer-Verlag, Berlin, pp. 247–269.

Nielsen, S.G., Mar-Gerrison, S., Gannoun, A., LaRowe, D.E., Klemm, V., Halliday, A., Burton, K.W., Hein, J.R., 2009. Thallium isotope evidence for increased marine organic carbon export in the early Eocene. Earth Planetary Science Letters *278*, 297–307.

Nielsen, S.G., Rehkämper, M., Prytulak, J., 2017. Investigation and application of thallium isotope fractionation. Reviews in Mineralogy and Geochemistry *82*, 759–798.

Och, L.M., Shields-Zhou, G.A., 2012. The Neoproterozoic oxygenation event: Environmental perturbations and biogeochemical cycling. Earth-Science Reviews *110*, 26–57.

Oehlert, A.M., Swart, P.K., 2014. Interpreting carbonate and organic carbon isotope covariance in the sedimentary record. Nature Communications *5*, 4672. doi:10.1038/ncomms5672.

Palmer, M.R., Pearson, P.N., Cobb, S.J., 1998. Reconstructing past ocean pH-depth profiles. Science *282*(5393), 1468–1471. doi:10.1126/science.282.5393.1468.

Papineau, D., Mojzsis, S.J., Karhu, J.A., Marty, B., 2005. Nitrogen isotopic composition of ammoniated phyllosilicates: Case studies from Precambrian metamorphosed sedimentary rocks. Chemical Geology *216*, 37–58.

Pasquier, V., Sansjofre, P., Rabineau, M., Revillon, S., Houghton, J., Fike, D.A., 2017. Pyrite sulfur isotopes reveal

glacial−interglacial environmental changes. Proceedings of the National Academy of Science *114*, 5941–5945. doi:10.1073/pnas.1618245114.

Pearson, P.N., van Dongen, B.E., Nicholas, C.J., Pancost, R.D., Schouten, S., Singano, J.M., Wade, B.S., 2007. Stable warm tropical climate through the Eocene Epoch. Geology *35*, 211–214.

Peckeur-Ehrenbrink, B., Ravizza, G., 2000. The marine osmium isotope record. Terra Nova *12*, 205–219.

Peckeur-Ehrenbrink, B., Ravizza, G., 2012. Osmium isotope stratigraphy. In: Gradstein, F.M., Ogg, J.G., Schmitz, M.D., Ogg, G.M. (Eds.), The Geologic Time Scale 2012. Elsevier, Amsterdam, Boston, vol. 1, chapter 8, pp. 145–166.

Peng, S., Babcock, L., Robison, R., Lin, H., Rees, M., Saltzman, M., 2004. Global Standard Stratotype-section and Point (GSSP) of the Furongian Series and Paibian Stage (Cambrian). Lethaia *37*, 365–379.

Penman, D.E., Hönisch, B., Zeebe, R.E., Thomas, E., Zachos, J.C., 2014. Rapid and sustained surface ocean acidification during the Paleocene–Eocene Thermal Maximum. Paleoceanography *29*, 357–369. doi:10.1002/2014PA002621.

Penniston-Dorland, S., Liu, X.M., Rudnick, R.L., 2017. Lithium isotope geochemistry. Reviews in Mineralogy and Geochemistry *82*, 165–217.

Percival, L.M.E., Witt, M.L.I., Mather, T.A., Hermoso, M., Jenkyns, H.C., Hesselbo, S.P., Al-Suwaidi, A.H., Storm, M.S., Xu, W., Ruhl, M., 2015. Globally enhanced mercury deposition during the end-Pliensbachian extinction and Toarcian OAE: A link to the Karoo–Ferrar Large Igneous Province. Earth and Planetary Science Letters *428*, 267–280.

Percival, L.M.E., Ruhl, M., Hesselbo, S.P., Jenkyns, H.C., Mather, T.A., Whiteside, J.H., 2017. Mercury evidence for pulsed volcanism during the end-Triassic mass extinction. Proceedings of the National Academy of Sciences of the United States of America *114*(30), 7929–7934. doi:10.1073/pnas.1705378114.

Petrizzo, D.A., Young, E.D., Runnegar, B.N., 2014. Implications of high-precision measurements of ^{13}C–^{18}O bond ordering in CO_2 for thermometry in modern bivalved mollusc shells. Geochimica et Cosmochimica Acta *142*, 400–410.

Pogge von Strandmann, P.A.E., Jenkyns, H.C., Woodfine, R.G., 2013. Lithium isotope evidence for enhanced weathering during Oceanic Anoxic Event 2. Nature Geoscience *6*, 668–672.

Pogge von Strandmann, P.A.E., Desrochers, A., Murphy, M.J., Finlay, A.J., Selby, D., Lenton, T.M., 2017. Global climate stabilisation by chemical weathering during the Hirnantian glaciation. Geochemical Perspectives Letters *3*(2), 230–237.

Pokrovsky, B.G., Mavromatis, V., Pokrovsky, O.S., 2011. Covariation of Mg and C isotopes in late Precambrian carbonates of the Siberian Platform: A new tool for tracing the change in weathering regime? Chemical Geology *290*, 67–74.

Poulton, S.W., Canfield, D.E., 2005. Development of a sequential extraction procedure for iron: Implications for iron partitioning in continentally derived particulates. Chemical Geology *214*, 209–221.

Poulton, S.W., Fralick, P.W., Canfield, D.E., 2004. The transition to a sulphidic ocean ~1.84 billion years ago. Nature *431*, 173–77.

Price, G.D., Mutterlose, J., 2004. Isotopic signals from late Jurassic–early Cretaceous (Volgian–Valanginian)sub-Arctic belemnites, Yatria River, Western Siberia. Journal of the Geological Society *161*, 959–968.

Puceat, E., Lecuyer, C., Sheppard, S.M.F., Dromart, G., Reboulet, S., Grandjean, P., 2003. Thermal evolution of Cretaceous Tethyan marine waters inferred from oxygen isotope composition of fish tooth enamels. Paleoceanography *18*(2), 1029. doi:10.1029/2002PA000823.

Railsback, L.B., Gibbard, P.L., Head, M.J., Voarintsoa, N.R.G., Toucanne, S., 2015. An optimized scheme of lettered marine isotope substages for the last 1.0 million years, and the climatostratigraphic nature of isotope stages and substages. Quaternary Science Reviews *111*, 94–106.

Ramkumar, M., 1999. Role of chemostratigraphic technique in reservoir characterization and global stratigraphic correlation. Indian Journal of Geochemistry *14*, 33–45.

Ramkumar, M., 2014. Characterization of depositional units for stratigraphic correlation, petroleum exploration and reservoir characterization. In: Sinha, S. (Ed.), Advances in Petroleum Engineering. Studium Press L.L.C, Houston, pp. 1–13.

Ramkumar, M., 2015. Toward standardization of terminologies and recognition of chemostratigraphy as a formal stratigraphic method. In: Ramkumar, M. (Ed.), Chemostratigraphy: Concepts, Techniques and Applications. Elsevier, Amsterdam, pp. 1–21. doi:10.1016/ B978-0-12-419968-2.00001-7.

Ramkumar, M., Stüben, D., Berner, Z., 2010. Hierarchical delineation and multivariate statistical discrimination of chemozones of the Cauvery Basin, South India: Implications on Spatio-temporal scales of stratigraphic correlation. Petroleum Science *7*, 435–447.

Ramkumar, M., Stüben, D., Berner, Z., 2011. Barremian–Danian chemostratigraphic sequences of the Cauvery Basin, South India: Implications on scales of stratigraphic correlation. Gondwana Research *19*, 291–309.

Ravizza, G., Peucker-Ehrenbrink, B., 2003. Chemostratigraphic evidence of Deccan Volcanism from the marine osmium isotope record. Science *302*, 1392–1395.

Ries, J.B., Fike, D.A., Pratt, L.M., Lyons, T.W., Grotzinger, J.P., 2009. Superheavy pyrite (δ34Spyr > δ34SCAS) in the terminal Proterozoic Nama Group, southern Namibia: A consequence of low seawater sulfate at the dawn of animal life. Geology *37*, 743–746.

Rodler, A.S., Frei, R., Gaucher, C., Germs, G.J.B., 2016. Chromium isotope, REE and redox-sensitive trace element chemostratigraphy across the late Neoproterozoic Ghaub glaciation, Otavi Group, Namibia. Precambrian Research *286*, 234–249.

Rodler, A., Frei, R., Gaucher, C., Korte, C., Rosing, S.A., Germs, G.J.B. 2017. Multiproxy isotope constraints on ocean compositional changes across the late Neoproterozoic Ghaub glaciation, Otavi Group, Namibia. Precambrian Research *298*, 306–324.

Saltzman, M.R., 2005. Phosphorus, nitrogen, and the redox evolution of the Paleozoic oceans. Geology *33*, 573–576.

Saltzman, M.R., Thomas, E., 2012. Carbon isotope stratigraphy. In: Gradstein, F.M., Ogg, J.G., Schmitz, M., Ogg, G.

(Eds.), The Geologic Time Scale. Elsevier, Amsterdam, Heidelberg. doi:10.1016/B978-0-444-59425-9.00011-1.

Salvador, A., 1994. International Stratigraphic Guide: A Guide to Stratigraphic Classification, Terminology and Procedure, 2nd Edition. IUGS-GSA, Boulder, pp. 1–214.

Sanei, H., Grasby, S.E., Beauchamp, B., 2012. Latest Permian mercury anomalies. Geology *40*, 63–66.

Sansjofre, P., Trindade R.I.F., Ader M., Soares, J.L., Nogueira A.C.R., Tribovillard, N., 2014. Paleoenvironment reconstruction of the Ediacaran Araras platform (Western Brazil) from the sedimentary and trace metals records. Precambrian Research *241*, 185–202.

Santos, G.M., Cordeiro, R.C., Silva Filho, E.V., Turcq, B., Lacerda, L.D., Fifield, L.K., Gomes, P.R.S., Hauscaden, P.A., Sifeddine, A., Albuquerque, A.L.S., 2001. Chronology of the atmospheric mercury in Lagoa da Pata Basin, Upper Rio Negro of Brazilian Amazon. Radiocarbon *43*, 801–808.

Sanyal, A., Bijma, J., Spero, H., David, H., Lea, W., 2001. Empirical relationship between pH and the boron isotopic composition of *Globigerinoides sacculifer* implications for the boron isotope paleo-pH proxy. Paleoceanography *16*, 515–519.

Sauzeat, L., Rudnick, R.L., Chauvel, C., Garcon, M., Tang, M., 2015. New perspectives on the Li isotopic composition of the upper continental crust and its weathering signature. Earth and Planetary Science Letters *428*, 181–192.

Sawaki, Y., Ohno, T., Tahata, M., Komiya, T., Hirata, T., Maruyama, S., Windley, B.F., Han, J., Shud, D., Li, Y., 2010. The Ediacaran radiogenic Sr isotope excursion in the Doushantuo Formation in the Three Gorges area, South China. Precambrian Research *176*, 46–64.

Scaife, J.D., Ruhl, M., Dickson, A.J., Mather, T.A., Jenkyns, H.C., Percival, L.M.E., Hesselbo, S.P., Cartwright, J., Eldrett, J.S., Bergman, S.C., Minisini, D., 2017. Sedimentary mercury enrichments as a marker for submarine Large Igneous Province volcanism? Evidence from the Mid-Cenomanian Event and Oceanic Anoxic Event 2 (Late Cretaceous). Geochemistry, Geophysics, Geosystems *18*(12), 4253–4275. doi:10.1002/2017GC007153.

Scheffler, K., Hoernes, S., Schwark, L., 2003. Global changes during Carboniferous–Permian glaciation of Gondwana: Linking polar and equatorial climate evolution by geochemical proxies. Geology *31*, 505–608.

Schidlowski, M., Hayes, J.M., Kaplan, I.R., 1983. Isotopic inferences of ancient biochemistries: Carbon, sulfur, hydrogen and nitrogen. In: Schopf, J.W. (Ed.), Earth's Earliest Biosphere: Its Origin and Evolution. Princeton University Press, Princeton, NJ, pp. 149–186.

Schmitz, B., Andersson, P., Dahl, J., 1988. Iridium, sulfur isotopes and rare earth elements in the Cretaceous-Tertiary boundary clay at Stevns Klint, Denmark. Geochimica et Cosmochimica Acta *52*(1), 229–236.

Schmitz, B., Pujalte, V., Molina, E., Monechi, S., Orue-Etxebarria, X., Speijer, R.P., Alegret, L., Apellaniz, E., Arenillas, I., Aubry, M.-P., Baceta, J.-I., Berggren, W.A., Bernaola, G., Caballero, F., Clemmensen, A., Dinarès-Turell, J., Dupuis, C., Heilmann-Clausen, C., Orús, A.H., Knox, R., Martín-Rubio, M., Ortiz, S., Payros, A., Petrizzo, M.R., von Salis, K., Sprong, J., Steurbaut, E., Thomsen, E., 2011. The global stratotype sections and points for the bases of the Selandian (Middle Paleocene) and Thanetian (Upper Paleocene Paleocene) stages at Zumaia, Spain. Episodes *34*, 220–243.

Scholle, P.A., Arthur, M.A. 1980. Carbon isotope fluctuations in Cretaceous pelagic limestones: Potential stratigraphic and petroleum exploration tool. American Association of Petroleum Geologists, Bulletin *64*, 67–87.

Scott, C., Lyons, T.W., Bekker, A., Shen, Y., Pultron, S.W., Chu, X., Anbar, A.D., 2008. Tracing the stepwise oxygenation of the Proterozoic ocean. Nature *452*, 456–459.

Scott, C.T., Bekker, A., Reinhard, C.T., Schnetger, B., Krapež, B., Rumble, D., Lyons, T.W., 2011. Late Archean euxinic conditions before the rise of atmospheric oxygen. Geology *39*(2), 119–122.

Shackleton, N.J., 1969. The last interglacial in the marine and terrestrial record. Proceedings of the Royal Society of London *174*, 135–154.

Shackleton, N.J., Opdyke, N.D., 1973. Oxygen isotope and palaeomagnetic stratigraphy of Equatorial Pacific core V28-238: Oxygen isotope temperatures and ice volumes on a 105 year and 106 year scale. Quaternary research *3*(1), 39–55.

Shackleton, N.J., Hall, M.A., 1984. Carbon isotope data from Leg 74 sediments. Initial Reports of the Deep Sea Drilling Project *74*, 613–619.

Sharma, M., Papanastassiou, D.A., Wasseburg, J., 1997. The concentration and isotopic composition of osmium in the oceans. Geochimica et Cosmochimica Acta *61*, 3287–3299.

Shen, Y., Knoll, A.H., Walter, M.R., 2003. Evidence for low sulphate and anoxia in a mid-Proterozoic marine basin. Nature *423*, 632.

Shields, G.A., 2007a. A normalised seawater strontium isotope curve and the Neoproterozoic-Cambrian chemical weathering event. Earth Discussions *2*, 69–84.

Shields, G., 2007b. The marine carbonate and chert isotope records and their implications for tectonics, life and climate on the early Earth. In: van Kranendonk, M.J., Smithies, R.H., Bennett, V.C. (Eds.), Earth's Oldest Rocks. Developments in Precambrian Geology *15*. Elsevier, Amsterdam, pp. 971–983.

Sial, A.N., Karhu, J., Ferreira, V.P., 2010a. Insights from isotope stratigraphy. Preface to the special issue on precambrian isotope stratigraphy. Precambrian Research *182*(4), v–viii.

Sial, A.N., Gaucher, C., Silva Filho, M.A., Ferreira, V.P., Pimentel, M.M., Lacerda, L.D., Silva Filho, E.V., Cezario, W., 2010b. C-, Sr-isotope and Hg chemostratigraphy of Neoproterozoic cap carbonates of the Sergipano Belt, Northeastern Brazil. In: Karhu, J., Sial, A.N., Ferreira, V.P. (Eds.), Precambrian Isotope Stratigraphy. Precambrian Research *182*. Elsevier, Amsterdam, pp. 351–372.

Sial, A.N., Lacerda, L.D., Ferreira, V.P., Frei, R., Marquillas, R.A., Barbosa, J.A., Gaucher, C., Windmöller, C.C., Pereira, N.S., 2013a. Mercury as a proxy for volcanic activity during extreme environmental turnover: The Cretaceous–Paleogene transition. Palaeogeography, Palaeoclimatology, Palaeoecology *387*, 153–164.

Sial, A.N., Chen, J.-B., Lacerda, L.D., Peralta, S., Gaucher, C., Frei, R., Cirilli, S., Ferreira, V.P., Marquillas, R.A., Barbosa, J.A., Pereira, N.S., Belmino, I.K.C., 2014. High-resolution

Hg chemostratigraphy: A contribution to the distinction of chemical fingerprints of the Deccan volcanism and Cretaceous–Paleogene Boundary impact event. Palaeogeography, Palaeoclimatology, Palaeoecology *414*, 98–115. doi:10.1016/j.palaeo.2014.08.013.

Sial, A.N., Gaucher, G., Ferreira, V.P., Pereira, N.S., Cezario, W.S., Chiglino, L., Monteiro, H., 2015a. Isotope and elemental chemostratigraphy. In: M. Ramkumar (Ed.), Chemostratigraphy, Concepts, Techniques and Applications. Elsevier, Amsterdam, pp. 23–64.

Sial, A.N., Campos, M.S., Gaucher, C., Frei, R., Ferreira, V.P., Nascimento, R.C., Pimentel, M.M., Pereira, N.S., Rodler, A., 2015b. Algoma-type Neoproterozoic BIFs and related marbles in the Seridó Belt (NE Brazil): REE, C, O, Cr and Sr isotope evidence. Journal of South American Earth Sciences *61*, 33–52.

Sial, A.N., Chen, J., Lacerda, L.D., Frei, R., Tewari, V.C., Pandit, M.K., Gaucher, C., Ferreira, V.P., Cirilli, S., Peralta, S., Korte, C., Barbosa, J.A., Pereira, N.S., 2016. Mercury enrichment and mercury isotopes in Cretaceous–Paleogene boundary successions: Links to volcanism and palaeoenvironmental impacts. Cretaceous Research *66*, 60–81. doi:10.1016/j.cretres.2016.05.006.

Sial, A.N., Chen, J., Lacerda, L.D., Frei, R., Tewari, V.C., Pandit, M.K., Gaucher, C., Ferreira, V.P., Cirilli, S., Peralta, S., Korte, C., Barbosa, J.A., Pereira, N.S., 2017. Reply to comments by Sanjay K. Mukhopadhyay, Sucharita Pal, J. P. Shrivastava on the paper by Sial et al. (2016) Mercury enrichments and Hg isotopes in Cretaceous–Paleogene boundary successions: Links to volcanism and palaeoenvironmental impacts. Cretaceous Research 66, 60–81. Cretaceous Research *78*, 84–88.

Sial, A.N., Chen, J., Lacerda, L.D., Frei, R., Higgins, J., Tewari, V.C., Gaucher, C., Ferreira, V.P., Cirilli, S., Peralta, S., Korte, C., Barbosa, J.A., Pereira, N.S., Ramos, D.S., this volume. Chemostratigraphy across the Cretaceous–Paleogene boundary. In: Sial, A.N., Gaucher, C., Ramkumar, M., Ferreira, V.P. (guest editors), Chemostratigraphy Across Major Chronological Eras. AGU/Wiley, United States.

Siebert, C., Nägler, T.F., von Blanckenburg, F., Kramers, J.D., 2003. Molybdenum isotope records as a potential new proxy for paleoceanography. Earth Planetary Science Letters *211*, 159–171.

Silva-Tamayo, J.C., Nägler, T.F., Villa, I.M., Kyser, K., Narbonne, G., James, N.P., Sial, A.N., Silva Filho, M.A., 2007. The aftermath of Snowball Earth: Ca- and Mo- isotope constraintson post-glacial ocean conditions. Geophysical Research Abstracts, *9*, 01980.

Silva Tamayo, J.C., Nägler, T., Villa, I.M., Kyser, K., Vieira, L.C., Sial, A.N., Narbonne, G.M., James, N.P., 2010a. Global Ca isotope variations in Post-Sturtian carbonate successions. Terra Nova *22*, 188–194.

Silva Tamayo, J.C., Nägler, T.F., Nogueira, A., Kyser, K., Villa, I., Riccomini, C., Sial, A.N., Narbonne, G.M., James, N.P., 2010b. Global perturbation of the marine Ca-isotopic composition in the aftermath of the Marinoan global glaciations. Precambrian Research *182*(4), 373–381.

Sluijs, A., Schouten, S., Donders, T.H., Schoon, P.L., Rohl, U., Reichart, G.-J., Sangiorgi, F., Kim, J.-H., Sinninghe Damste, J.S., Brinkhuis, H., 2009. Warm and wet conditions in the Arctic region during Eocene Thermal Maximum 2. Nature Geosciences *2*, 777–780.

Sosa-Montes, C., Rodríguez-Tovar, F.J., Martínez-Ruiz, F., Monaco, C.P., 2017. Paleoenvironmental conditions across the Cretaceous–Paleogene transition at the Apennines sections (Italy): An integrated geochemical and ichnological approach. Cretaceous Research *71*, 1–13. doi:10.1016/j.cretres.2016.11.005.

Spangenberg, J.E., Bagnoud-Velásquez, M., Boggiani, P.C., Gaucher, C., 2014. Redox variations and bioproductivity in the Ediacaran: Evidence from inorganic and organic geochemistry of the Corumbá Group, Brazil. Gondwana Research *26*, 1186–1207.

Staubwasser, M., Von Blackenburg, F., Shoenberg, R., 2006. Iron isotopes in the early marine diagenetic iron cycle. Geology *34*, 629–632.

Steinhoefel, G., von Blanckenburg, F., Horn, I., Konhauser, K.O., Beukes, N.J., Gutzmer, J., 2010. Deciphering formation processes of banded iron formations from the Transvaal and the Hamersley successions by combined Si and Fe isotope analysis using UV femtosecond laser ablation. Geochimica et Cosmochimica Acta *74*, 2677–2696.

Steininger, F.F., Aubry, M.P., Berggren, W.A., Biolzi, M., Borsetti, A.M., Cartlidge, J.E., Cati, F., Corfield, R., Gelati, R., Iaccarino, S., Napoleone, C., Ottner, F., Rögl, F., Roetzel, R., Spezzaferri, S., Tateo, F., Villa, G., Zevenboom, D., 1997. The Global Stratotype Section and Point (GSSP) for the base of the Neogene. Episodes *20*, 23–28.

Strandmann, P.A.E., Forshaw, J., Schmidt, D.N., 2014. Modern and Cenozoic records of seawater magnesium from foraminiferal Mg isotopes. Biogeosciences *11*, 5155–5168.

Strauss, H., 1997. The isotopic composition of sedimentary sulfur through time. Paleogeography, Palaeoclimatology, Palaeoecology *132*, 97–118.

Sundquist, E.T., Visser, K., 2004. The geologic history of the carbon cycle. Treatise on Geochemistry *8*, 425–472.

Tahata, M., Ueno, Y., Ishikawa, T., Sawaki, Y., Murakami, K., Han, J., Shu, D., Li, Y., Guo, J., Yoshida, N., Komiya, T., 2013. Carbon and oxygen isotope chemostratigraphies of the Yangtze platform, South China: Decoding temperature and environmental changes through the Ediacaran. Gondwana Research *23*(1), 333–356. doi:10.1016/j.gr.2012.04.005.

Teng, F.-Z., Watkins, J.M., Dauphas, N., 2017. Non-traditional stable isotopes. Reviews in Mineralogy and Geochemistry *82*, 885 pp.

Thibodeau, A.M., Bergquist, B.A., 2017. Do mercury isotopes record the signature of massive volcanism in marine sedimentary records? Geology *45*, 95–96.

Thibodeau, A.M., Ritterbush, K., Yager, J.A., West, A.J., Ibarra, Y., Bottjer, D.J., Berelson, W.M., Bergquist, B.A., Corsetti, F.A., 2016. Mercury anomalies and the timing of biotic recovery following the end-Triassic mass extinction. Nature Communications *7*, 1–8.

Tipper, E.T., Bickle, M.J., Galy, A., West, J., Pomiés, C., Chapman, H.J., 2006a. The short term sensitivity of carbonates and silicate weathering fluxes: Insight from seasonal variations in river chemistry. Geochimica et Cosmochimica Acta *70*, 2737–2754.

Tipper, E.T., Galy, A., Bickle, M.J., 2006b. Riverine evidence for a fractionated reservoir of Ca and Mg on the continents: Implications for the oceanic Ca cycle. Earth Planetary Science Letters *247*, 267–279.

Tipper, E.T., Galy, A., Gaillardet, J., Bickle, M.J., Elderfield, H., Carder, E.A., 2006c. The magnesium isotope budget of the modern ocean: Constraints from riverine magnesium isotope ratios. Earth Planetary Science Letters *250*, 241–253.

Tipper, E.T., Louvat, P., Capmas, F., Galy, A., Gaillardet, J., 2008. Accuracy of stable Mg and Ca isotope data obtained by MC-ICP-MS using the standard addition method. Chemical Geology *257*, 65–75.

Tomascak, P.B., Magna, T.S., Dohmen, R., 2016. Advances in Lithium Isotope Geochemistry. Springer International Publishing, Cham, 195 pp.

Tribovillard, N., Algeo, T.J., Lyons, T., Riboulleau, A., 2006. Trace metals as paleoredox and paleoproductivity proxies: An update. Chemical Geology *232*, 12–32.

Tribovillard, N., Algeo, T.J., Baudin, F., Riboulleau, A., 2012. Analysis of marine environmental conditions based on molybdenum-uranium covariation-applications to Mesozoic paleoceanography. Chemical Geology *324/325*, 46–58.

Tripati, A., Eagle, R., Thiagarajan, N., Gagnon, A., Bauch, H., Halloran, P., Eiler, J., 2010. ^{13}C–^{18}O isotope signatures and "clumped isotope" thermometry in foraminifera and coccoliths. Geochimica et Cosmochimica Acta *74*, 5697–5717.

Vandenbroucke, T.R.A., Armstrong, H.A., Williams, M., Paris, F., Zalasiewicz, J.A., Sabbe, K., Nolvak, J., Challandsa, T.J., Verniers, J., Servais, T., 2010. Polar front shift and atmospheric CO_2 during the glacial maximum of the Early Paleozoic Icehouse. Proceedings of the National Academy of Sciences of the United States of America *107*, 14983–14986.

Van de Schootbrugge, B., Bachan, A., Suan, G., Richoz, S., Payne, J.L., 2013. Microbes, mud and methane: Cause and consequence of recurrent Early Jurassic anoxia following the end-Triassic mass extinction. Paleontology *56*, 1–25. doi:10.1111/pala.120341.

Veizer, J., Holser, W.T., Wilgus, C.K., 1980. Correlation of $^{13}C/^{12}C$ and $^{34}S/^{32}S$ secular variations. Geochimica Cosmochimica Acta *44*, 579–588.

Veizer, J., Compston, W., Clauer, N., Schidlowski, M., 1983. $^{87}Sr/^{86}Sr$ in late Proterozoic carbonates: Evidence for a "mantle" event at approximately 900 Ma ago. Geochimica et Cosmochimica Acta *47*, 295–302.

Veizer, J., Ala, D., Azmy, K., Bruckschen, P., Buhl, P., Bruhn, F., Carden, G.A.F., Diener, A., Ebneth, S., Godderis, Y., Jasper, T., Korte, C., Pawellek, F., Podlaha, O.G., Strauss, H., 1999. $^{87}Sr/^{86}Sr$, $\delta^{13}C$ and $\delta^{18}O$ evolution of Phanerozoic seawater. Chemical Geology *161*, 59–88.

Vennemann, T.W., Hegner, E., 1998. Oxygen, strontium, and neodymium isotope composition of fossil shark teeth as a proxy for the palaeoceanography and palaeoclimatology of the Miocene northern Alpine Paratethys. Palaeogeography, Palaeoclimatology, Palaeoecology *142*, 107–121.

Walker, M., Johnsen, S., Rasmussen, S.O., Popp, T., Steffensen, J.-P., Gibbard, P., Hoek, W., Lowe, J., Andrews, J., Rck, S.B., Cwynar, L.C., Hughen, K., Kershaw, P., Kromer, B., Litt, T., Lowe, D.J., Nakagawa, T., Newnham, R., Schwander, J., 2009. Formal definition and dating of the GSSP (Global Stratotype Section and Point) for the base of the Holocene using the Greenland NGRIP ice core, and selected auxiliary records. Journal of Quaternary Science *24*, 3–17.

Wen, H., Fan, F., Zhang, Y., Cloquet, C.,Carignan, J., 2015. Reconstruction of early Cambrian ocean chemistry from Mo isotopes. Geochimica et Cosmochimica Acta *164*, 1–16.

Williams, D.F., Thunell, R.C., Tappa, E., Rio, D., Raffi, I. 1988. Chronology of the Pleistocene oxygen isotope record: 0–1.88 my BP. Palaeogeography, Palaeoclimatology, Palaeoecology *64*(3–4), 221–240.

Wombacher, F., Eisenhauer, A., Heuser, A., Weyer, S., 2009. Separation of Mg, Ca and Fe from geological reference materials for stable isotope ratio analyses by MC-ICP-MS and double-spike TIMS. Journal Analytical Atomic Spectrometry *24*, 627–636.

Wombacher, F., Eisenhauer, A., Böhm, F., Gussone, N., Regenberg, M., Dullo, W.-C., Rüggeberg, A., 2011. Magnesium stable isotope fractionation in marine biogenic calcite and aragonite. Geochimica Cosmochica Acta *75*, 5797–5818.

Xu, C., Rong, J., Fan, J., Zhan, R., Mitchell, C.E., Harper, D.A.T., Melchin, M.J., Peng, P., Finney, S.C., Wang, X., 2006. The Global Boundary Stratotype Section and Point (GSSP) for the base of the Hirnantian Stage (the uppermost of the Ordovician System). Episodes *2*, 183–196.

Yu, J., Elderfield, H., 2007. Benthic foraminiferal B/Ca ratios reflect deep water carbonate saturation state. Earth and Planetary Science Letters *258*, 73–86.

Zachos, J., Pagani, M., Sloan, L., Thomas, E., Billups, K., 2001. Trends, rhythms, and aberrations in global climate 65 Ma to present. Science *292*, 686–693.

Zachos, J.C., Schouten, S., Bohaty, S., Quattlebaum, T., Sluijs, A., Brinkhuis, H., Gibbs, S.J., Bralower, T.J., 2006. Extreme warming of mid-latitude coastal ocean during the Paleocene-Eocene Thermal Maximum: Inferences from TEX86 and isotope data. Geology *34*, 737–740.